(1)

Semiannual Technical Report

Low Temperature Deposition and Characterization of N- and P-Type Silicon Carbide Thin Films and Associated Ohmic and Schottky Contacts

Supported under Grant #N00014-92-J-1500
Office of the Chief of Naval Research
Report for the period 1/1/94–6/30/94

R. F. Davis and R. J. Nemanich*
M. C. Benjamin*, S. Kern, L. M. Porter, and S. Tanaka
Materials Science and Engineering Department
*Department of Physics
North Carolina State University
Raleigh, NC 27695

June, 1994

REPORT DOCUMENTATION PAGE

Form Approved
OMB No. 0704-0188

1. AGENCY USE ONLY (Leave blank)	2. REPORT DATE	3. REPORT TYPE AND DATES COVERED
	June, 1994	Semiannual Technical 1/1/94–6/30/94

4. TITLE AND SUBTITLE
Low Temperature Deposition and Characterization of N- and P-Type Silicon Carbide Thin Films and Associated Ohmic and Schottky Contacts

5. FUNDING NUMBERS
sic0002---02
1261
N00179
N66005
4B855

6. AUTHOR(S)
Robert F. Davis and Robert J. Nemanich

7. PERFORMING ORGANIZATION NAME(S) AND ADDRESS(ES)
North Carolina State University
Hillsborough Street
Raleigh, NC 27695

8. PERFORMING ORGANIZATION REPORT NUMBER
N00014-92-J-1500

9. SPONSORING/MONITORING AGENCY NAMES(S) AND ADDRESS(ES)
Sponsoring: ONR, Code 1261, 800 N. Quincy, Arlington, VA 22217-5660
Monitoring: Office of Naval Research Resider
The Ohio State University Research Center
1960 Kenny Road
Columbus, OH 43210-1063

10. SPONSORING/MONITORING AGENCY REPORT NUMBER

11. SUPPLEMENTARY NOTES

12a. DISTRIBUTION/AVAILABILITY STATEMENT
Approved for Public Release; Distribution Unlimited

12b. DISTRIBUTION CODE

13. ABSTRACT (Maximum 200 words)

Monocrystalline silicon carbide (SiC) films have been grown on vicinal 6H-SiC (0001) substrates via gas source molecular beam epitaxy at 1050–1250°C. Using transmission electron microscopy, step bunching was observed at the outset of the initial stage of growth using C_2H_4/Si_2H_6 ratios of 1, 2 or 10. Subsequent growth occurred via island formation (C_2H_4-rich) or step-flow (1:1 ratio). Occurrence of the different growth modes may be controlled by changes in the surface diffusion length caused by surface reconstruction as a result of changing the C/Si ratio. Cubic β-SiC and hexagonal 6H-SiC deposit using high and 1:1 C/Si ratios, respectively. Unintentionally doped films are n-type with $n = (0.2–1.0)\times10^{17}$ cm^{-3}. Similar atomic and hole concentrations of 5×10^{18} and 1.2×10^{18}, respectively, were measured in Al-doped p-type films. AlN deposited on 6H-SiC (0001) substrates possess a negative electron affinity. The surface Fermi level of the AlN is ~3.5 eV above the valence band maximum. Thin film electrical contacts of Co exhibited rectifying behavior with $n<1.06$ and a leakage current of 2.0×10^{-8} at -10 V. After annealing at 1000°C for 2 min, ohmic-like behavior was observed as a result of significant interface reaction.

14. SUBJECT TERMS
6H-SiC, β-SiC, AlN, molecular beam epitaxy, thin films, surface reconstruction, step bunching, island growth, step-flow growth, C_2H_4/Si_2H_6 ratios, n-type, p-type, Co, rectifying contact, ohmic contact, annealing

15. NUMBER OF PAGES
43

16. PRICE CODE

17. SECURITY CLASSIFICATION OF REPORT	18. SECURITY CLASSIFICATION OF THIS PAGE	19. SECURITY CLASSIFICATION OF ABSTRACT	20. LIMITATION OF ABSTRACT
UNCLAS	UNCLAS	UNCLAS	SAR

Table of Contents

I. Introduction

Silicon carbide (SiC) is a wide bandgap material that exhibits polytypism, a one-dimensional polymorphism arising from the various possible stacking sequences of the silicon and carbon layers. The lone cubic polytype, β-SiC, crystallizes in the zincblende structure and is commonly referred to as 3C-SiC. In addition, there are also approximately 250 other rhombohedral and hexagonal polytypes [1] that are all classed under the heading of α-SiC. The most common of the α-SiC polytypes is 6H-SiC, where the 6 refers to the number of Si/C bilayers along the closest packed direction in the unit cell and the H indicates that the crystal structure is hexagonal.

Beta (3C)-SiC is of considerable interest for electronic applications that utilize its attractive physical and electronic properties such as wide bandgap (2.2 eV at 300K) [2], high breakdown electric field (2.5×10^6 V/cm) [3], high thermal conductivity (3.9 W/cm °C) [4], high melting point (3103K at 30 atm) [5], high saturated drift velocity (2×10^7 m/s) [6], and small dielectric constant (9.7) [7]. Primarily due to its higher electron mobility than that of the hexagonal polytypes, such as 6H-SiC [8], β-SiC remains preferable to hexagonal SiC for most device applications.

Most 3C-SiC thin film growth to date has been performed on Si substrates. Large-area, crack-free, and relatively thick (up to 30 μm) epitaxial 3C-SiC thin films have been grown on Si (100) by exposing the Si substrate to a C-bearing gaseous species prior to further SiC growth [7, 9, 10]. However, these films exhibited large numbers of line and planar defects due to large lattice and thermal mismatches between SiC and Si. One particular type of planar defect, the inversion domain boundary (IDB), was eliminated with the use of Si (100) substrates cut 2°–4° toward [011] [11–13]. Growth on Si substrates has allowed much understanding of SiC growth processes and device development to occur, but the large thermal and lattice mismatches between SiC and Si hamper further development using Si substrates. As a result, great effort has been made to develop methods for growth SiC single crystal substrates for homoepitaxial growth of SiC thin films.

Since the 1950's, monocrystalline single crystals of 6H-SiC have been grown at using the Lely sublimation process [14]. However, nucleation was uncontrolled using this process and control of resultant polytypes was difficult. SiC single crystals inadvertently formed during the industrial Acheson process have also been used as substrates for SiC growth. However, neither these crystals or those formed using the Lely process are large enough for practical device applications. Recently, using a seeded sublimation-growth process, boules of single polytype 6H-SiC of > 1 inch diameter of much higher quality of that obtained using the Lely process have been grown. The use of single crystals of the 6H polytype cut from these boules has given a significant boost to SiC device development.

Silicon carbide epitaxial thin film growth on hexagonal SiC substrates has been reported since the 1960's. The use of nominally on-axis SiC substrates has usually resulted in growth of 3C-SiC films. Films of 3C-SiC (111) grown by CVD have been formed on 6H-SiC substrates less than 1° off (0001) [15]. Films of 3C-SiC on 6H-SiC substrates have typically had much lower defect densities than those grown on Si substrates. The major defects present in 3C-SiC/6H-SiC films have been double positioning boundaries (DPB) [16]. Despite the presence of DPBs, the resultant material was of sufficient quality to further device development of SiC. The use of off-axis 6H-SiC (0001) substrates has resulted in growth of high-quality monocrystalline 6H-SiC layers with very low defect densities [17].

In addition, the use of more advanced deposition techniques, such as molecular beam epitaxy (MBE), has been reported for SiC in order to reduce the growth temperature and from about 1400–1500°C on 6H-SiC substrates. Si and C electron-beam sources have been used to epitaxially deposit SiC on 6H-SiC (0001) at temperatures of 1150°C [18]. Ion-beam deposition of epitaxial 3C-SiC on 6H-SiC has also been obtained at the temperature of 750°C using mass-separated ion beams of $^{30}Si^{+}$ and $^{13}C^{+}$ [19].

Aluminum nitride (AlN) is also of particular interest at this time because of its very large bandgap. It is the only intermediate phase in the Al-N system and normally forms in the wurtzite (2H-AlN) structure. Most current uses of AlN center on its mechanical properties, such as high hardness (9 on Mohs scale), chemical stability, and decomposition temperature of about 2000°C [20]. Properties such as high electrical resistivity (typically $\geq 10^{13}$ Ω-cm), high thermal conductivity (3.2 W/cm K) [21], and low dielectric constant ($\varepsilon \approx 9.0$) make it useful as a potential substrate material for semiconductor devices as well as for heat sinks. The wurtzite form has a bandgap of 6.28 eV [22] and is a direct transition, thus it is of great interest for optoelectronic applications in the ultraviolet region.

Because of the difference in bandgaps (2.28 eV for 3C-SiC and 6.28 eV for 2H-AlN) between the materials, a considerable range of wide bandgap materials, made with these materials, should be possible. Two procedures for bandgap engineering are solid solutions and multilayers. A particularly important factor is that the two materials have a lattice mismatch of less than one percent.

Research in ceramic systems suggests that complete solid solubility of AlN in SiC may exist [23]. Solid solutions of the wurtzite crystal structure should have E_g from 3.33 eV to 6.28 eV at 0 K. Although it has not been measured, the bandgap of cubic AlN has been estimated to be around 5.11 eV at absolute zero and is believed to be indirect [24]. Cubic solid solutions should thus have E_g from 2.28 eV to roughly 5.11 eV at 0 K and would be indirect at all compositions if theory holds true.

Because of their similarity in structure and close lattice and thermal match, AlN-SiC heterostructures are feasible for electronic and optoelectronic devices in the blue and infrared

region. Monocrystalline AlN layers have been formed by CVD on SiC substrates [25] and SiC layers have been formed on AlN substrates formed by AlN sputtering on single crystal W [26]. In addition, theory on electronic structure and bonding at SiC/AlN interfaces [24] exists and critical layer thicknesses for misfit dislocation formation have been calculated for cubic AlN/SiC [27]. Note that AlN (at least in the wurtzite structure) is a direct-gap material and SiC is an indirect gap material. Superlattices of these materials would have a different band structure than either constituent element. The Brillouin zone of a superlattice in the direction normal to the interfaces is reduced in size. This reduction in zone size relative to bulk semiconductors causes the superlattice bands to be "folded into" this new, smaller zone. This folding can cause certain superlattice states to occur at different points in k space than the corresponding bulk material states [28]. This can lead to direct transitions between materials which in the bulk form have indirect transitions. This has been demonstrated in the case of $GaAs_{0.4}P_{0.6}$/GaP and $GaAs_{0.2}P_{0.8}$/GaP superlattices, where both constituents are indirect in the bulk form [29]. Whether this is possible in the case of AlN/SiC is unknown, but very intriguing. It may be possible to obtain direct transitions throughout nearly the entire bandgap range with use of superlattices of AlN and SiC. Use of solid solutions in superlattices introduces additional degrees of freedom. For example, the bandgap can be varied independently of the lattice constant with proper choice of layer thickness and composition if superlattices of solid solutions of AlN and SiC were formed.

Due to the potential applications of solid solutions and superlattice structures of these two materials, an MBE/ALE system was commissioned, designed, and constructed for growth of the individual compounds of SiC and AlN, as well as solid solutions and heterostructures of these two materials. Dithisimal studies concerned with the kinetics and mechanisms of mass transport of Si, C, Al and N at the SiC/AlN interface are also being conducted in tandem with the deposition investigations.

A very important additional goal of this research is to understand what controls the contact electrical characteristics of specific metals to n-type 6H-SiC and to use this information to form good ohmic and Schottky contacts. A list of five metals to be studied, which consists of Ti, Pt, Hf, Co, and Sr, was created at the beginning of this research project. The selection process began by taking the simplest case, an ideal contact which behaves according to Schottky-Mott theory. This theory proposes that when an intimate metal-semiconductor contact is made the Fermi levels align, creating an energy barrier equal to the difference between the workfunction of the metal and the electron affinity of the semiconductor. It is the height of this barrier which determines how the contact will behave; for ohmic contacts it is desirable to have either no barrier or a negative barrier to electron flow, while for a good Schottky contact a large barrier is desired.

Although metals were chosen optimistically, i.e. on the basis that they will form ideal contacts, some evidence exists that the contact properties will be more complicated. J. Pelletier *et al.* [30] have reported Fermi level pinning in 6H-SiC due to intrinsic surface states, suggesting little dependence of barrier height on the workfunction of the metal. In addition, L. J. Brillson [31, 32] predicts the pinning rate to be higher for more covalently bonded materials. Other complications may arise if the surface is not chemically pristine. A major part of this project will be devoted to determining whether the contacts behave at all ideally, and if not, whether the Fermi level is pinned by intrinsic or extrinsic effects.

Along with examining the barriers of the pure metal contacts, the chemistry upon annealing will be studied and correlated with the resulting electrical behavior. The electrical behavior will be quantified both macroscopically in terms of current-voltage characteristics and micro-scopically in terms of barrier height. Identification of the phases formed will present the opportunity to attribute the electrical characteristics to the new phase in contact with silicon carbide.

Within this reporting period, investigations concerned with (1) the determination of the effect of the C_2H_4/Si_2H_6 ratio of the mode of growth of SiC on 6H-SiC wafers and the polytype of film which formed, (2) the n-and p-type doping of the SiC films, (3) the controlled deposition of AlN films on SiC and vice-versa, (4) the determination of negative electron affinity effects in AlN and (4) the deposition of Co contacts and their annealing have been conducted. Island formation and step-flow growth modes and surface reconstruction occurred as a function of the C_2H_4/Si_2H_6 ratio. Unintentionally doped SiC films are n-type with n = (0.2 - 1.0)$\times 10^{17}$ cm^{-3}. Similar atomic and hole concentrations of 5×10^{18} and 1.2×10^{18}, respectively, were measured in Al-doped p-type films. Thin film electrical contacts of Co exhibited rectifying behavior with n<1.06 and a leakage current of 2.0×10^{-8} at -10 V. After annealing at 1000°C for 2 min, ohmic-like behavior was observed as a result of significant interface reaction.

The experimental procedures, results, discussion of these results, conclusions and plans for future efforts for each of the topics noted above are presented in the following sections. Each of these sections is self-contained with its own figures, tables and references.

References

1. G. R. Fisher and P. Barnes, Philos. Mag. B **61**, 217 (1990).
2. H. P. Philipp and E. A. Taft, in *Silicon Carbide, A High Temperature Semiconductor*, edited by J. R. O'Connor and J. Smiltens (Pergamon, New York, 1960), p. 371.
3. W. von Muench and I. Pfaffender, J. Appl. Phys. **48**, 4831 (1977).
4. E. A. Bergemeister, W. von Muench, and E. Pettenpaul, J. Appl. Phys. **50**, 5790 (1974).
5. R. I. Skace and G. A. Slack, in *Silicon Carbide, A High Temperature Semiconductor*, edited by J. R. O'Connor and J. Smiltens (Pergamon, New York, 1960), p. 24.
6. W. von Muench and E. Pettenpaul, J. Appl. Phys. **48**, 4823 (1977).

7. S. Nishino, Y. Hazuki, H. Matsunami, and T. Tanaka, J. Electrochem Soc. **127**, 2674 (1980).
8. P. Das and K. Ferry, Solid State Electronics **19**, 851 (1976).
9. K. Sasaki, E. Sakuma, S. Misawa, S. Yoshida, and S. Gonda, Appl. Phys. Lett. **45**, 72 (1984).
10. P. Liaw and R. F. Davis, J. Electrochem. Soc. **132**, 642 (1985).
11. K. Shibahara, S. Nishino, and H. Matsunami, J. Cryst. Growth **78**, 538 (1986).
12. J. A. Powell, L. G. Matus, M. A. Kuczmarski, C. M. Chorey, T. T. Cheng, and P. Pirouz, Appl. Phys. Lett. **51**, 823 (1987).
13. H. S. Kong, Y. C. Wang, J. T. Glass, and R. F. Davis, J. Mater. Res **3**, 521 (1988).
14. J. A. Lely, Ber. Deut. Keram. Ges. **32**, 229 (1955).
15. H. S. Kong, J. T. Glass, and R. F. Davis, Appl. Phys. Lett. **49**, 1074 (1986).
16. H. S. Kong, B. L. Jiang, J. T. Glass, G. A. Rozgonyi, and K. L. More, J. Appl. Phys. **63**, 2645 (1988).
17. H. S. Kong, J. T. Glass, and R. F. Davis, J. Appl. Phys. **64**, 2672 (1988).
18. S. Kaneda, Y. Sakamoto, T. Mihara, and T. Tanaka, J. Cryst. Growth **81**, 536 (1987).
19. S. P. Withrow, K. L. More, R. A. Zuhr, and T. E. Haynes, Vacuum **39**, 1065 (1990).
20. C. F. Cline and J. S. Kahn, J. Electrochem. Soc, **110**, 773 (1963).
21. G. A. Slack, J. Phys. Chem. Solids **34**, 321 (1973).
22. W. M. Yim, E. J. Stofko, P. J. Zanzucci, J. I. Pankove, M. Ettenberg, and S. L. Gilbert, J. Appl. Phys. **44**, 292 (1973).
23. See, for example, R. Ruh and A. Zangvil, J. Am. Ceram. Soc. **65**, 260 (1982).
24. W. R. L. Lambrecht and B. Segall, Phys. Rev. B **43**, 7070 (1991).
25. T. L. Chu, D. W. Ing, and A. J. Norieka, Solid-State Electron. **10**, 1023 (1967).
26. R. F. Rutz and J. J. Cuomo, in *Silicon Carbide-1973*, ed. by R. C. Marshall, J. W. Faust, Jr., and C. E. Ryan, Univ. of South Carolina Press, Columbia, p. 72 (1974).
27. M. E. Sherwin and T. J. Drummond, J. Appl. Phys. **69**, 8423 (1991).
28. G. C. Osbourn, J. Vac. Sci. Technol. B **1**, 379 (1983).
29. P. L. Gourley, R. M. Biefeld, G. C. Osbourn, and I. J. Fritz, *Proceedings of 1982 Int'l Symposium on GaAs and Related Compounds* (Institute of Physics, Berkshire, 1983), p. 248.
30. J. Pelletier, D. Gervais, and C. Pomot, J. Appl. **55**, 994 (1984).
31. L. J. Brillson, Phys. Rev. B **18**, 2431 (1978).
32. L. J. Brillson, Surf. Sci. Rep. **2**, 123 (1982).

II. Effects of Gas Flow Ratio on the Growth Mode of Silicon Carbide by Gas-source Molecular Beam Epitaxy

A. Introduction

Since silicon carbide possesses a wide band gap (2.9 eV), high saturated electron drift velocity (2×10^7 cm/s), high breakdown field (5×10^6 V/cm), high thermal conductivity (3.5 W/cm°C at 300K), and chemical stability, it has been extensively studied for high temperature, high-power, and high-frequency electronic device applications [1]. Besides its superior electrical properties, SiC has an unique crystallographic characteristic, namely extensive *polytypism* [2]. The difference in stacking sequences of the close-packed planes, $(111)_{cubic}$ or $(0001)_{hexagonal}$, can form more than 250 different polytypes. The 3C (β), 6H, and 4H are most popular polytypes due to their energetic and kinetic stability in nature. Although their formation mechanisms are not yet known, their film growth has been conducted by several methods, such as chemical vapor deposition [3, 4] and molecular beam epitaxy [5, 6]. In terms of homoepitaxial growth of SiC, which can result in a higher film quality due to the lack of lattice mismatch and other effects such as in SiC/Si system, the film polytype can be generally determined by the substrate polytype, if the growth mode is 'step flow'[3]. Step flow can be kinetically achieved when adatoms reach the step sites and retain the identical stacking sequence as the substrate. Therefore, 6H films can be formed on 6H SiC substrate with the presence of steps at relatively lower growth temperatures of <1500°C where 3C is normally the more stable polytype [7].

Step flow growth has been achieved by CVD in the range of growth temperatures of 1200°C-1600°C to produce 6H and 4H homoepitaxial films [3, 4, 8]. The growth mechanisms of CVD deposited films investigated through kinetic [9] and microstructural [10] considerations. On the other hand, SiC film growth by MBE at lower growth temperatures (<1200°C) on 6H-SiC substrates has not fully been successful. Yoshinobu *et al.* has grown 3C films on either 6H-SiC $(000\bar{1})$ [5] and 3C-SiC(001) [11] substrates at <1000°C by an alternating supply of Si_2H_6 and C_2H_2. However, a simultaneous supply of each gas caused either no film or polycrystalline island growth below 1100°C.

In this paper, we have successfully grown 6H-SiC films on vicinal 6H-SiC (0001) substrate at 1050°C by a simultaneous supply of source gases. The effects of gas flow ratios of C_2H_4/Si_2H_6 on growth mode was investigated. We found that the ethylene-rich conditions can cause islanding and that step flow growth can be achieved by a 1:1 ratio. Considering the surface chemistry, reconstruction, and related adatom diffusivities through the observation of the initial stage of growth by HRTEM and *in-situ* RHEED, a growth model is discussed.

B. Experimental Procedure

Silicon carbide films were typically grown on Si-faces of 6H-SiC (0001) substrates. The substrates used in this study were off-axis (3-4° off (0001) toward <11$\bar{2}$0>) provided by Cree Research, Inc.[14] Films were all grown by a GSMBE method under varying conditions. The typical growth conditions are listed in Table I. Note that all depositions were performed at 1050°C. The detail description of the deposition technique can be found in Ref. 6. The as-received substrates were dipped in 10% HF solution for 5 min. to remove the protective surface oxide layer (typically ~750Å), immediately followed by loading into the MBE system. Each substrate was annealed at 1050°C in the ultra high vacuum environmental (~1×10^{-9} torr) for 30 min. prior to the deposition in order to remove residual hydrocarbons and surface oxides. During the depositions, RHEED patterns were monitored by the use of a charge coupled device camera and video recorder. After growing the film, the sample was cut and glued face to face to make a cross-sectional TEM sample, followed by the standard sample preparation techniques [13]. Finally, the sample was examined by a Topcon EM-OO2B operated at a 200kV acceleration voltage with the use of the <$\bar{2}$110> zone axis.

Table I. Typical Growth Conditions for the SiC Films

Temperature	1050°C
Se_2H_6 flow rate	0.1 sccm
C_2H_4 flow rate	0.1-1.0 sccm
C_2H_4/Si_2H_6 flow ratio	1.0, 2.0, 10.0
Growth rate	50-100Å/hr

C. Results and Discussion

Figure 1 shows the cross-sectional image of the SiC film on an off-axis (vicinal) 6H-SiC (0001) substrate. The resulting film was generally cubic (3C) in structure and had a rough surface morphology due to island growth under the condition of a ratio of $C_2H_4/Si_2H_6 = 2$. The islands (3C) which nucleated on the different terrace sites and are separated by steps (indicated by the arrows) can be clearly seen. The more ethylene-rich condition of $C_2H_4/Si_2H_6 = 10$ showed the similar features of $C_2H_4/Si_2H_6 = 2$ condition except the density of the islands decreased. Moreover, it can be observed that there are steps which are 1/2 to 2 unit cell height (c = 15Å). According to the preliminary investigation of vicinal 6H-SiC surface structure by HRTEM, monolayer (consisting of Si and C layers) steps predominantly exist on the surface [14]. Thus, this implies the occurrence of step bunching at the early stage

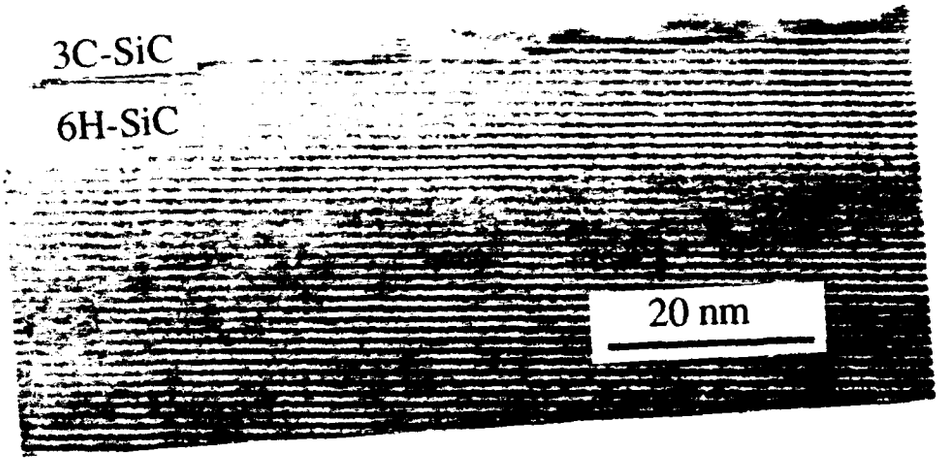

Figure 1. TEM image of 3C island growth at $C_2H_4/Si_2H_6 = 2$.

of growth. At the early stage of growth where monolayer steps are available (accordingly terrace width is ~60Å), the adatoms can migrate to the step site to cause step flow because of the comparable diffusion length of the adatoms to terrace width. It should be emphasized here that step bunching can substantially be observed if the difference in diffusivities of the (000n) planes of 6H-SiC where n=1 to 6 is present. Interestingly, energetic calculations by Heine *et. al* [7] can provide the difference in surface energies, showing the lowest energy plane is A in the ABC notation. Thus, the presence of step bunching at the early stage of growth can be reasonable. As the terrace width increases, adatoms can not reach the step sites to retain step flow due to the limited diffusion length at the growth temperature, and ultimately islands form on the terrace site. During the growth of both films, RHEED initially showed a streaky (1×1) pattern and changed to a spotty (1×1) pattern which was indicative of 3C island formation and included double positioning boundaries (DPBs) [15]. The details of the RHEED study will be reported in the future.

Under the different condition in which $C_2H_4/Si_2H_6 = 1$, a dramatic change in the film growth mode was observed. Figure 3 (a) shows 6H-SiC film growth with a stepped surface. At present the film growth rate is not verified, however, it is very positive that 6H-SiC film growth could be performed under these conditions. Because the stepped surface feature is

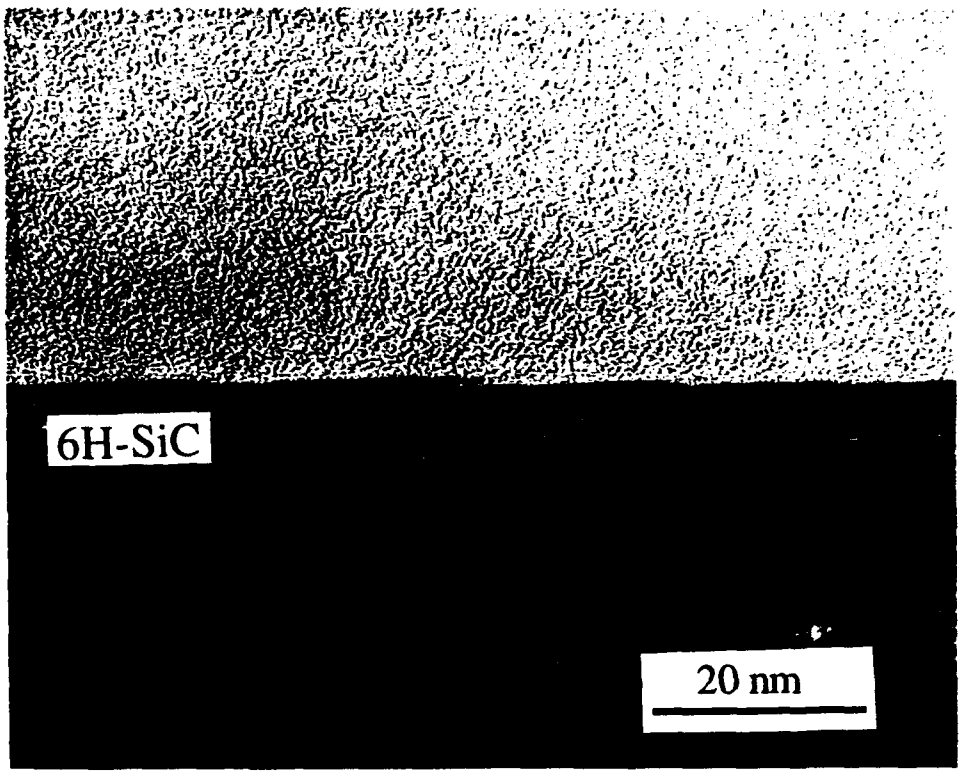

Figure 2. TEM image of step flow growth at $C_2H_4/Si_2H_6 = 1$.

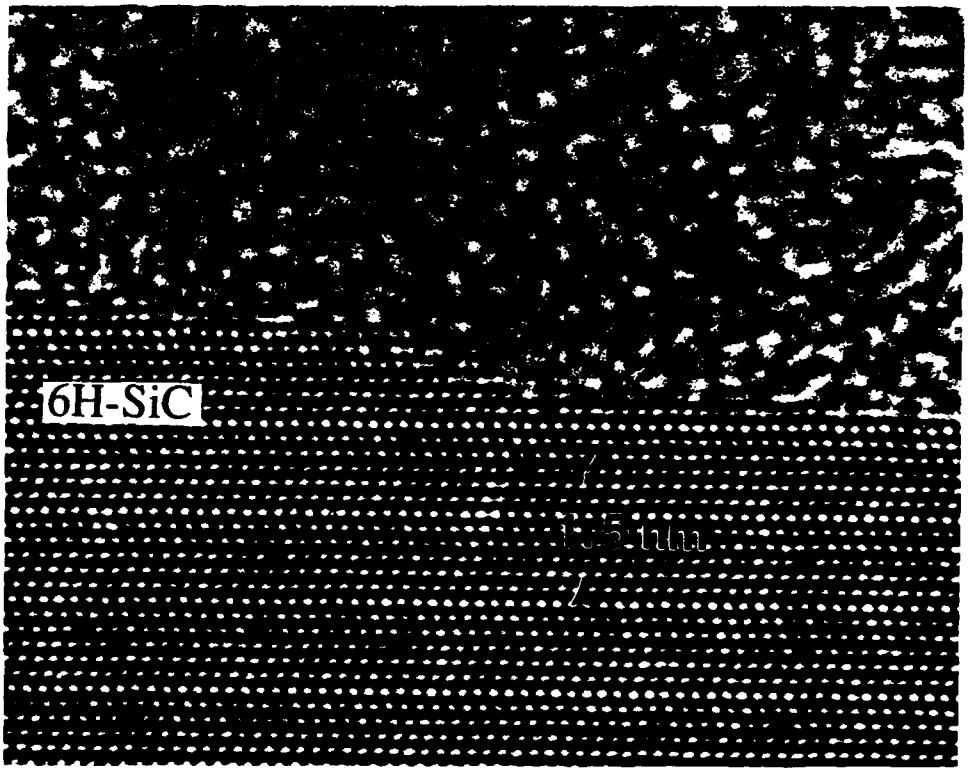

Figure 3. HRTEM image of the stepped surface occurred by step flow growth at $C_2H_4/Si_2H_6 = 1$.

apparently different from that of the substrate surface as mentioned in the previous paragraph. In Fig. 3 (b), a magnified image of the stepped surface is shown. A step having a half unit cell height (3~4 monolayers) clearly indicates step flow growth. During the film growth, (3×3) reconstruction was observed by RHEED as shown in Fig. 4. Kaplan proposed the model for this reconstruction [16], consisting of an adsorbed Si bilayer.

Figure 4. (3×3) RHEED pattern observed during the growth of the SiC film at $C_2H_4/Si_2H_6 = 1$.

We have recognized that the gas flow ratio of C_2H_4/Si_2H_6 influenced the growth mode significantly with step bunching plus island formation and step flow under ethylene rich (= 2 and 10) and 1:1 conditions, respectively. As indicated by the RHEED patterns, the (3×3) surface reconstruction occurred under the condition of $C_2H_4/Si_2H_6 = 1$, suggesting the lower surface energy of the growing surface. Thus, the surface mobilities of adatoms can be enhanced to some degree on such a reconstructed surface, leading a step flow growth.

D. Conclusion

In summary, we have successfully grown 6H-SiC films on 6H-SiC substrates by GSMBE utilizing a simultaneous supply of source gases at a relatively low temperature of 1050°C. Step flow growth was enhanced under the condition of $C_2H_4/Si_2H_6 = 1$ possibly due to the surface reconstruction during growth which introduced the higher mobility of adatoms. Under the different gas flow ratios such as $C_2H_4/Si_2H_6 = 2$ and 10, step bunching plus islanding was observed.

E. Future Plans

HRTEM and *in-situ* RHEED will continue to be used in studying the growth mechanisms. The growth mechanisms which has been established in this report will be investigated in more details through *in-situ* RHEED oscillation and a scanning tunneling

microscope at Oak Ridge National Laboratory. Preliminary observation of the very early stage of SiC growth showed the plausibility of the model established in this study. More quantitative discussion will be desired in terms of surface mobilities of adatoms on the reconstructed surfaces and growing surface chemistry. The control of polytype formation (2H and 4H) will be also challenged on the basis of the theory obtained in this study.

F. References

1. R. F. Davis, Physica B **185**, 1 (1993).
2. N. W. Jepps and T. F. Page, Progress in Crystal Growth and Characterization **7**, edited by P. Krishna (Pergamon Press, New York, 1983), 259.
3. H. S., Kong, J. T. Glass, and R. F. Davis, J. Appl. Phys **64**, 2672 (1988).
4. H. Matsunami, T. Ueda, and H. Nishino, Mater. Res. Soc. Symp. Proc. **162**, 397 (1990).
5. T. Yoshinobu, M. Nakayama, H. Shimoi, T. Fuyuki, and H. Matsunami, J. Cryst. Growth **99**, 520 (1990).
6. L. B. Rowland, R. S. Kern, S. Tanaka, and R. F. Davis, J. Mater. Res. **8**, 2753 (1993).
7. V. Heine, C. Chen, and R. J. Needs, J. Am. Ceram. Soc. **74**, 2630 (1991).
8. T. Kimoto, A. Yamashita, A. Itoh, and H. Matsunami, Jpn. J. Appl. Phys. **32**, 1045 (1993).
9. T. Kimoto, H. Nishino, W. S. Yoo, and H. Matsunami, J. Appl. Phys. **73**, 726 (1993).
10. F. R. Chien, S. R. Nutt, W. S. Yoo, T. Kimoto, and H. Matsunami, J. Mater. Res. **9**, 940 (1994).
11. T. Yoshinobu, H. Mitsui, I. Izumikawa, T. Fuyuki, and H. Matsunami, Appl. Phys. Lett. **60**, 824 (1992).
12. Cree Research Inc., Durham, NC.
13. C. H. Carter, Jr., R. F. Davis, and S. R. Nutt, J. Mater. Res. **1**, 811 (1986).
14. unpublished
15. L. B. Rowland, R. S. Kern, S. Tanaka, and R. F. Davis, Appl. Phys. Lett. **62**, 3333 (1993).
16. R. Kaplan, Surf. Sci. **215**, 111 (1989).

III. Growth and Characterization of Thin, Epitaxial Silicon Carbide Films by Gas-source Molecular Beam Epitaxy

A. Introduction

Interest in wide band gap semiconductor materials for use in high-temperature, -power, -frequency and -speed microelectronic devices resistant to radiation has escalated on a global scale within the last decade. Silicon carbide (SiC) is one of the leading candidate materials fueling this interest. This material occurs in a number of different structural variants called polytypes that arise as a result of the different stacking sequences of the Si/C bilayers along the directions of closest packing. There is one cubic polytype (β- or 3C-SiC) and approximately 250 hexagonal and rhombohedral polytypes that are collectively denoted as α-SiC. The most common of these is 6H-SiC. Many electronic properties, including band gap, are dependent on the polytype.

Thin film growth of 3C- and 6H-SiC has been achieved primarily via chemical vapor deposition (CVD) (see Davis *et al.* [1] for a review of this and related research). Monocrystalline Si wafers have been the principal substrate of choice for 3C deposition. This is achieved by a carbonization step in which a C-containing gas converts the Si(100) surface to 3C-SiC to reduce the effects of the large mismatches in lattice parameters (≈20%) and coefficients of thermal expansion (≈10%). The epitaxial growth of SiC films on α(6H)-SiC(0001) substrates via CVD has been reported for three decades [1]. When the [0001] direction of the 6H wafer is oriented off-axis ≤0.5°, the result is single phase β-SiC films [2,3]. Double positioning boundaries (DPB) are the primary defects in these films [4]. Deposition at T≥1400°C on substrates cut 3-4° towards [11$\bar{2}$0] have resulted in high-quality monocrystalline 6H-SiC layers with low defect densities [5,6].

Solid- and gas-source (GS) molecular beam epitaxy (MBE) techniques have also been employed for deposition of SiC films on a variety of substrates. All previous researchers achieved the growth of only β-SiC. The best results for lower defect densities have been obtained on 6H-SiC substrates. Kaneda *et al.* [7] studied the relationships between the ratio of fluxes of electron-beam evaporated Si and C and the temperature of the on-axis α(6H)-SiC{0001} substrates in the range of 1150-1400°C. Stoichiometric, epitaxial 3C-SiC(111) films were obtained at particular source flux ratios ($J_{Si}/J_C \geq 1$) between 1150-1400°C. No information was given by these authors regarding the substrate face, the microstructure of the resultant films or the type of defects present in these films; however, they were able to fabricate p-n junctions by adding B to the solid Si source. Rowland *et al.* [8] deposited β-SiC(111) on vicinal α(6H)-SiC(0001) at 1050°C using 0.5 standard cubic centimeters per minute (sccm) Si_2H_6 and 2.0 sccm C_2H_4. The resulting films grew primarily as islands on the terraces between steps resulting in films with a high DPB density. By

contrast, Yoshinobu *et al.* [9] employed the periodic introduction of Si_2H_6 and C_2H_2 to achieve 3C-SiC growth on vicinal 6H-SiC(000$\bar{1}$) and 6H-SiC(0$\bar{1}$1$\bar{4}$) substrates at 850-1160°C. Films grown on vicinal 6H-SiC(000$\bar{1}$) contained DPBs while those grown on 6H-SiC(0$\bar{1}$1$\bar{4}$) were free of these defects. Smooth films were obtained at the lowest growth rates used in the study (< 0.01 μm/hr).

B. Experimental Procedure

In the present research, SiC films were grown using a specially designed and previously described [10] GSMBE system. The base and operating pressures were 10^{-9} Torr and 10^{-3}-10^{-6} Torr, respectively. All films were grown between 1050–1250°C using 1:1 ratios of disilane (Si_2H_6, 99.99% purity) and ethylene (C_2H_4, 99.99% purity) with total source inputs ranging from 0.6-4.0 sccm on off-axis α(6H)-SiC(0001) and thin 2H-AlN(0001) buffer layers on on-axis α(6H)-SiC(0001). The thin AlN layers were grown for 1 minute in the same system at 1050°C using a standard Al (99.9999% purity) effusion cell source, operating at 1260°C, and a compact electron cyclotron resonance (ECR) source to activ.. 3.5 sccm of N_2 (99.9995% purity). (This procedure has been described previously [11, 12]). Solid aluminum, evaporated from a standard MBE effusion cell, was used for p-type doping. Substrates were chemically cleaned prior to growth in a 10% HF solution for 5 minutes, loaded immediately into the growth chamber and then evacuated to ultrahigh vacuum. A surface pretreatment step, in which the substrates were heated to 1050°C and held for 10 minutes, exposed to a 1 sccm flux of Si_2H_6 for minute and heated to 1200°C to evaporate the Si from the surface, was performed prior to growth. The surface of the substrates was monitored using reflection high-energy diffraction (RHEED) operating at 10 kV.

RHEED was also used to determine the crystalline quality and structure of the surface of the resulting films. High-resolution transmission electron microscopy (HRTEM), operating at 200 kV, was employed to observe the microstructure of the film as well as film/substrate interfaces. Secondary ion mass spectrometry (SIMS), using 10 keV O^+ ions, was employed to determine the atomic concentration of Al. Carrier concentrations for undoped SiC films, grown on insulating AlN layers, and p-type doped films were measured at room temperature by standard Hall techniques at 3.5 kG. Nickel contacts, RF sputtered at room temperature then annealed at 1000°C for 30 s in Ar, were used on the undoped films and aluminum contacts, evaporated at room temperature and annealed at 500°C for 30 seconds in Ar, were used on p-type films.

C. Results

Film Growth. Figure 1 shows a representative HRTEM image of a homoepitaxial, undoped 6H-SiC film on a 6H-SiC(0001) substrate cut 3-4° towards [1$\bar{2}$0]. This la.. was

grown for 2 hours at 1250°C using 1.0 sccm Si_2H_6 and 1.0 sccm C_2H_4. The lattice fringes seen in the image are indicative of the 6H stacking sequence. Although it is very difficult to determine the thickness of such a thin, undoped film, the thickness is expected to be about 1200 Å based on previously determined growth rates.

Figure 2 shows a HRTEM micrograph of a 3C-SiC/2H-AlN/6H-SiC heterostructure. The SiC layer was grown on approximately 1.5 nm of AlN on an on-axis 6H-SiC(0001) substrate at 1050°C for 1 hour using 0.3 sccm Si_2H_6 and 0.3 sccm C_2H_4. Similar to previous report of growth on AlN [12, 13], the resulting SiC film is of the 3C polytype. Hall electric characterization on thicker SiC films (≈0.5 μm) grown under the same conditions for longer times revealed the films to have carrier concentrations on the order of 2×10^{16} cm^{-3}-1×10^{17} cm^{-3}.

Figures 3a and 3b show RHEED photographs taken along major poles on the two SiC films described above. The photograph in Fig. 3a, taken along the [$11\bar{2}0$] azimuth of the film shown in Fig. 1, is indicative of a smooth 6H-SiC film. Figure 3b, showing the [110] azimuth of the SiC surface of the multilayer film shown in Fig. 2, shows a typical pattern for a smooth surface of 3C-SiC.

Film Doping. Carrier concentrations were measured on a number of Al-doped 6H-SiC films by the Hall technique. These films were grown under the same conditions as in Fig. 1. Four different doping levels were achieved with Al effusion cell temperatures held at 700°C, 800°C, 900°C and 1000°C. The results are shown in Table I. As expected, the carrier concentration increased as the effusion cell temperature was increased.

Table I. Measured Carrier Concentrations in Various P-type SiC Films

Aluminum Cell Temperature (°C)	Carrier Concentration from Hall Measurements (cm^{-3})
700	3.8×10^{16}*
800	5.3×10^{16}
900	8.2×10^{17}
1000	1.2×10^{18}

* Sespite apparent Al incorporation, this film is still n-type according to Hall and Hot Probe analysis.

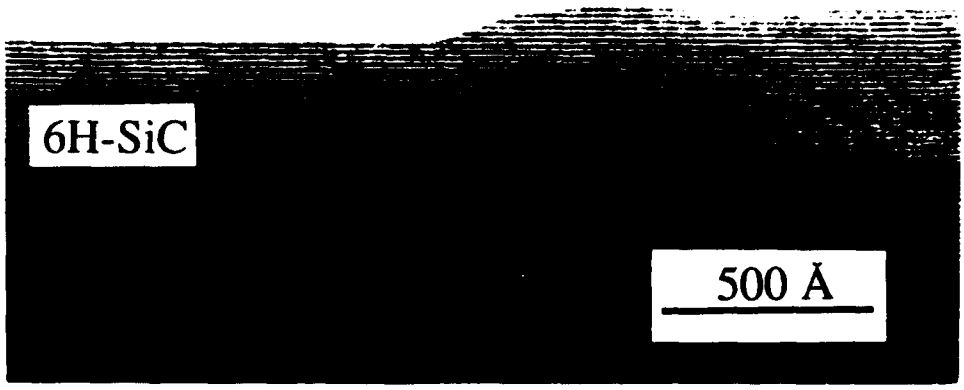

Figure 1. HRTEM micrograph of a homoepitaxial, undoped 6H-SiC(0001) film grown on a vicinal 6H-SiC(0001) substrate. Note the very large step and the wide, smooth terrace that results.

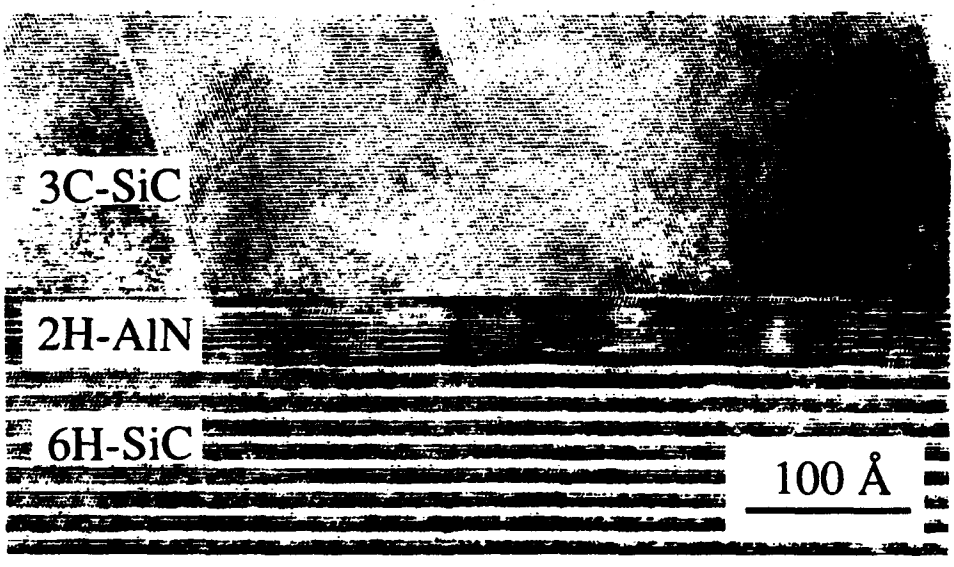

Figure 2. HRTEM micrograph of a 3C-SiC(111) film on a thin (≈1.5 nm) 2H-AlN(0001) layer grown on on-axis 6H-SiC(0001). Note the smooth 3C-SiC layer that results.

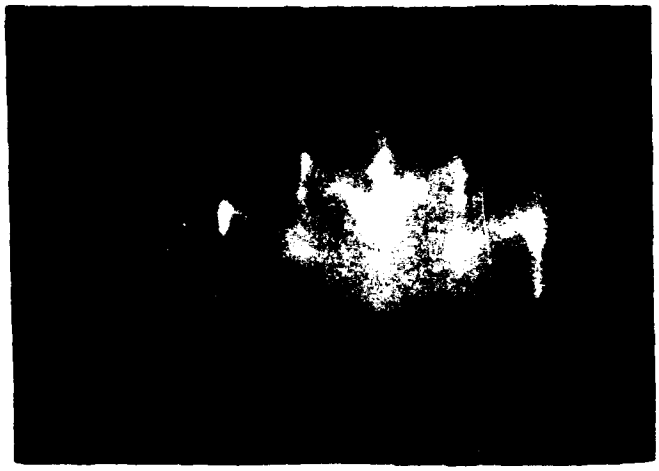

(a)

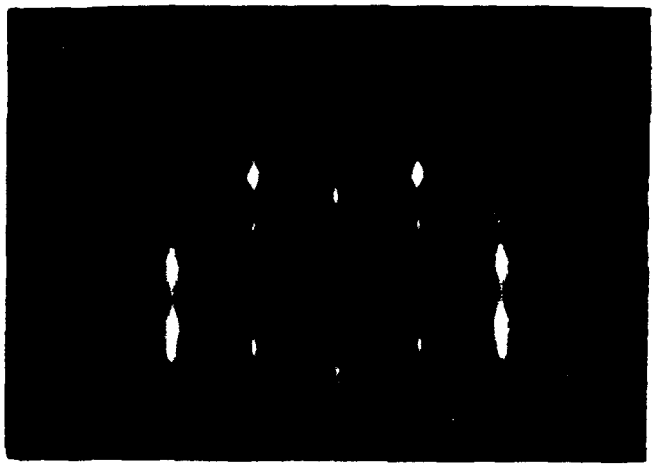

(b)

Figure 3. RHEED photographs of (a) the 6H-SiC film shown in Fig. 1 and (b) the 3C-SiC film shown in Fig. 2.

Figure 4 shows SIMS profiles for the same p-type films as displayed in Table I. The film having the lowest Al doping, and labeled as 700°C, is at the Al detection limit of 5×10^{15} cm^{-3} for the instrument. The highest doped of these films shows a very non-uniform profile due to occasional Al inclusions, observed as bright spots in the sputtering crater, within the film.

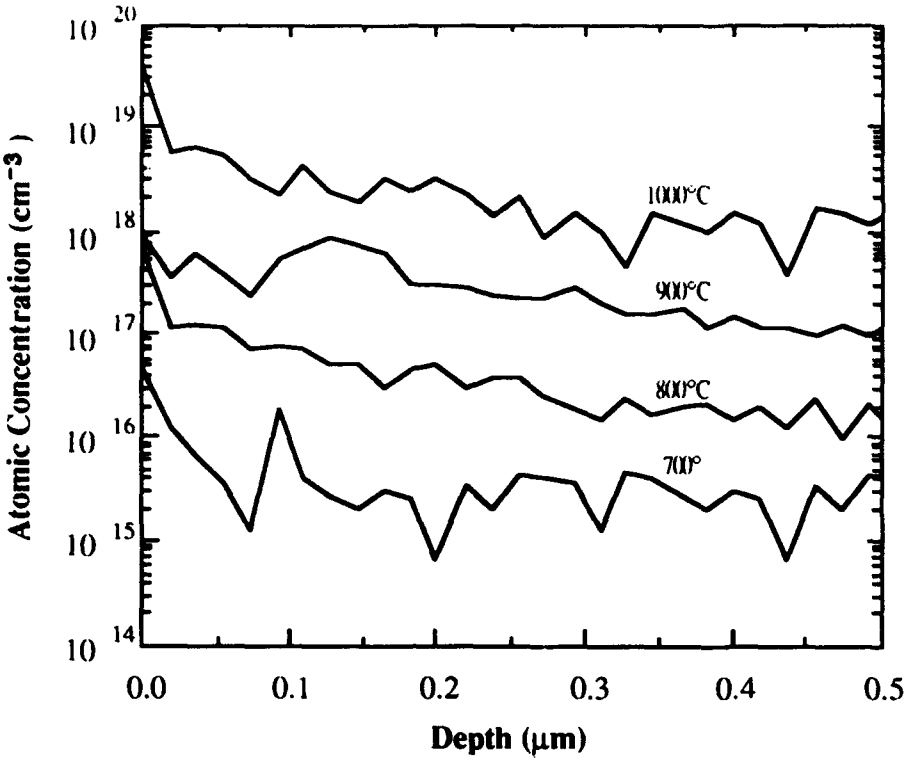

Figure 4. SIMS profiles for 6H-SiC films doped with Al from an MBE effusion cell at different source temperatures.

D. Discussion

The large surface step (≈15 nm or 10 unit cells) seen in Fig. 1 is most likely the result of a combination of step flow and step bunching during growth whereby different steps, which have different surface energies associated with them, grow laterally at different velocities until they impinge on one another [14]. By contrast, the majority of the film is extremely smooth with widely spaced steps. Although not yet suitable for device applications, this film represents a significant step toward that goal.

The film shown in Fig. 2 and the resulting electrical data from similarly produced films represent the best β-SiC(111) produced by this system. The role of the AlN buffer layer is not fully understood, but this film appears much smoother and less defective than 3C layers grown directly on 6H substrates [8,9].

The Hall measurements listed in Table I and the SIMS data displayed in Fig. 4 represent one of the first attempts at SiC doping by MBE. As expected, the concentration of both impurity atoms and carriers increased as the source flux increased. The high levels of Al seen at the surface in the SIMS plot are probably a result of ineffective shuttering of the solid Al source at the conclusion of growth. Gas sources can be immediately diverted to another pump but the solid source can only be shuttered while the flux decreases during cooling. This was a particular problem and a possible source of the Al inclusions observed on the

surface of the highest doped films. These profiles and the data from Table I are the same order of magnitude indicating a much higher activation efficiency than previously reported by CVD [15].

E. Conclusions

Films of 3C- and 6H-SiC have been grown between 1050-1250°C by GSMBE using Si_2H_6 and C_2H_4 on different orientations of α(6H)-SiC(0001) and on thin buffer layers of AlN. Growth of SiC on AlN represents a possible means of growing higher quality β-SiC(111) than previously reported. Hall electrical measurements on these films revealed carrier concentration of 2×10^{16} cm^{-3}–1×10^{17} cm^{-3}.

Doped films of 6H-SiC have been grown on vicinal α(6H)-SiC(0001) at 1250°C. The films (doped p-type with Al) showed atomic Al concentrations varied with increasing Al effusion cell temperature. These films showed carrier concentrations between 5.3×10^{16} and 1.2×10^{18} with the lowest Al incorporation only partially compensating the as-grown n-type character. SIMS profiles for Al incorporation are of the same order of magnitude indicating a much higher activation efficiency than previously reported by CVD.

F. Future Research Plans and Goals

Further study of SiC growth will center on the basic requirements necessary to produce device structures. These include increasing growth rate, a full understanding of polytype control, and both p- and n-type doping. In addition, studies are underway to examine the role of the thin AlN buffer layer and the relatively high dopant activation efficiency. The lone system modification necessary may be a redesign of the shuttering mechanism.

G. References

1. R. F. Davis, J. W. Palmour and J. A. Edmond, Diamond and Related Materials **1**, 109 (1992).
2. H. S. Kong, J. T. Glass and R. F. Davis, Appl. Phys. Lett. **49**, 1074 (1986).
3. K. Shibahara, N. Kuroda, S. Nishino and H. Matsunami, Jpn. J. Appl. Phys. **26**, L1815 (1987).
4. H. S. Kong, B. L. Jiang, J. T. Glass, G. A. Rozgonyi and K. L. More, J. Appl. Phys. **63**, 2645 (1988).
5. H. S. Kong, J. T. Glass and R. F. Davis, J. Appl. Phys. **64**, 2672 (1988).
6. N. Kuroda, K. Shibahara, W. Yoo, S. Nishino and H. Matsunami, in *Extended Abstracts of the 19th Conference on Solid State Devices and Materials* (Business Center for Academic Societies, Tokyo, 1987), p. 227.
7. S. Kaneda, Y. Sakamoto, T. Mihara and T. Tanaka, J. Cryst. Growth **81**, 536 (1987).
8. L. B. Rowland, R. S. Kern, S. Tanaka and R. F. Davis, J. Mater. Res., **8**, 2753 (1993).
9. T. Yoshinobu, H. Mitsui, I. Izumikawa, T. Fuyuki and H. Matsunami, Appl. Phys. Lett. **60**, 824 (1992).

10. L. B. Rowland, S. Tanaka, R. S. Kern and R. F. Davis, in *Proceedings of the Fourth International Conference on Amorphous and Crystalline Silicon Carbide and Related Materials*, edited by C. Y. Yang, M. M. Rahman and G. L. Harris (Springer-Verlag, Berlin, 1992) p. 84.
11. L. B. Rowland, R. S. Kern, S. Tanaka and R. F. Davis, J. Mater. Res. **8**, 2310 (1993).
12. L. B.Rowland, R. S. Kern, S. Tanaka and R. F. Davis, Appl. Phys. Lett. **62**, 3333 (1993).
13. R. S. Kern, S. Tanaka, and R. F. Davis, to be published in *Proceedings of the International Conference on Sicon Carbide and Related Materials.*
14. F. R. Chien, S. R. Nutt, W. S. Yoo, T. Kimoto and H. Matsunami, J. Mat. Res. **9**, 940 (1994).
15. H. J. Kim and R. F. Davis, J. Electrochem. Soc. **133**, 2350 (1986).

IV. Properties of the Heteroepitaxial AlN/SiC Interface

A. Introduction

The semiconductor industry is presently limited in device application by the materials used in device fabrication. Novel materials are being sought to replace Si- and Ge-based devices. Devices are needed which operate at higher temperatures, powers, and frequencies than before. Radiation hardness is also a valued trait. Potential materials are diamond, SiC, AlN, and GaN. These wide bandgap semiconductors have the properties needed to realize these goals. Of these materials, SiC appears most advantageous [1]. This material can be readily grown and working devices have been made of SiC [2].

The material studied was an aluminum nitride (AlN) film grown epitaxially on a 6H silicon carbide (SiC) substrate. AlN has a direct optical band gap of 6.2 eV and a wurtzite hexagonal structure with an a-axis lattice constant of 3.11 Å. The growth was achieved by molecular beam epitaxy (MBE). The epitaxial growth is confirmed by RHEED measurements [3]. SiC can be used as a substrate for the growth of AlN due to the close lattice match (3.08Å vs. 3.11Å). This allows for the manufacturing of novel structures such as Negative Electron Affinity (NEA) surfaces for UV and X-ray detectors and cold cathode emitters. The possibility for NEA based vacuum collector-emitters also exists [4]. The phenomenon of a negative electron affinity (NEA) occurs at a semiconductor surface when the vacuum energy level lies below the conduction band edge. Since the bonding of common semiconductors are based on sp^3 hybridization, the valance band develops from bonding levels and the conduction band from the antibonding atomic orbitals. Since wide band gap semiconductors have common bonding origin, the NEA phenomenon is more likely to occur for these materials. The consequence of a NEA surface is that any electrons from the valence band promoted into the conduction band can escape from the material. Thus, having an NEA surface enhances cathode operation (emission).

B. Experimental Procedure

The presence of a NEA can be determined by ultraviolet photoemission spectroscopy (UPS) [5-7]. This technique involves directing 21.2 eV light (the He I resonance line) to the surface of the sample and detecting the spectrum of the emitted photo excited electrons as a function of electron kinetic energy. Typically, UPS is used to obtain a profile of the valence band (VB) electronic states. As such, most studies of UPS of semiconductors present data of the most energetic electrons emitted from the surface. Electrons scattered to lower energy and secondary electrons will be displayed in the spectra at lower kinetic energies. In addition, for a semiconductor which exhibits a NEA surface, a distinctive peak may be observed at the low kinetic energy (highest binding energy) end of the photoemission spectra. Fig. 1 depicts a

schematic representation of the photoemission spectra from a semiconductor with a negative or positive electron affinity. The low kinetic energy feature is due to secondary electrons which (quasi) thermalize to the conduction band minimum.

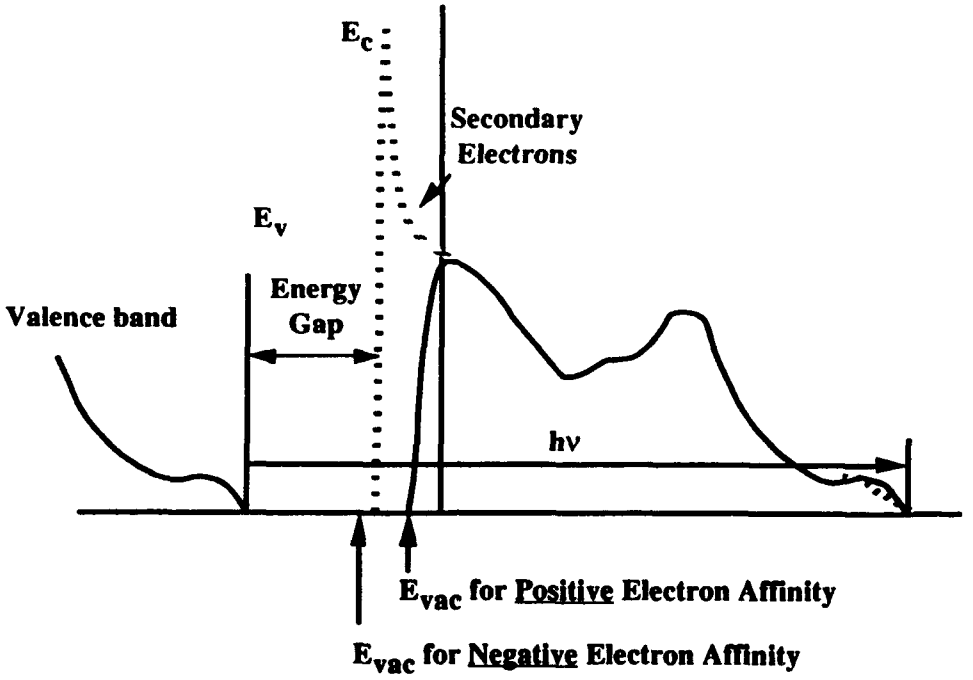

Figure 1. A schematic of the difference in the photoemission spectra of a semiconductor with a positive or negative electron affinity.

The sharp features typical of a NEA have been observed from spectra of (111) and (100) diamond surfaces [5-9]. In the studies of diamond, a correlation was made between the presence of hydrogen and the NEA peak [6,7]. In addition, it was also shown that thin metal layers such as Ti or other low workfunction metals could induce a NEA on the diamond surface [9,10]. These measurements verify that the surface dipole can be influenced by surface processing and that the effects contribute to the observation of a NEA.

For the AlN UPS studies presented here, the SiC substrate is important for two reasons. The first is that from wide bandgap semiconductors there would be charging problems, and the photoemission would be quickly quenched. The reason for this is that, with such a large band gap, the AlN acts as an insulator and will charge up. This problem is avoided by growing a thin layer of AlN on a conducting doped SiC substrate. The n-type SiC substrates used in this study, being more conductive than bulk AlN, provide a source of electrons for photoemission. The second benefit of the SiC substrate is the small lattice mismatch between SiC and AlN (3.08 Å vs. 3.11 Å). The small lattice mismatch enables heteroepitaxial growth.

The AlN/SiC sample was deposited on the SiC substrate by a modified gas source MBE system. The substrate was a vicinal wafer of 6H polytype (0001) (oriented 3-4 degrees towards [1120]) SiC which resulted in the growth of hexagonal (2H) AlN. The MBE system consists of three parts: a load lock (base pressure of 5×10^{-8} Torr), a transfer tube (base pressure of 1×10^{-10} Torr), which also was used for degassing the substrates, and the growth chamber (base pressure of 5×10^{-11} Torr). Knudson effusion cells with BN crucibles and Ta wire heaters were charged with 6N pure aluminum. Ultra-high purity nitrogen, further purified by a chemical purifier, was used as the source gas. The nitrogen gas was excited by an ECR plasma source, which was designed to fit inside the 2.25 inch diameter tube of the source flange cryoshroud. The details of the system can be found elsewhere. [11]

The SiC substrates were obtained from Cree Research Inc. Prior to loading into the chamber, the substrates were cleaned by a standard degreasing and RCA cleaning procedure. After undergoing a degassing procedure in UHV (700 °C for 30 minutes), the substrates were transferred into the deposition chamber. Epitaxial AlN films were deposited under the conditions shown below in Table I. The films examined were roughly 100 Å thick.

Table I. Deposition Conditions for MBE AlN Film Growth

Nitrogen pressure:	2×10^{-4} Torr
Microwave power:	50W
Aluminum cell temp:	1120 °C
Substrate temperature:	1100 °C
Deposition Rate:	1000Å/hr

The samples were transported in air to the surface analysis system. The analysis system is made up of several chambers linked by a linear UHV transfer line. The details of the system are described elsewhere [8,10]. Among the capabilities available are UPS, XPS, LEED, hydrogen and argon plasma cleaning, thermal programmed desorption, and Auger Spectroscopy.

The UPS chamber has a base pressure of 2×10^{-10} Torr. Operating conditions involve pressures up to 1×10^{-9} Torr, but the higher pressure is due to the helium inflow and does not contaminate the sample. The UPS system utilizes a helium resonance lamp (the He I line) to provide a source of 21.2 eV light. Photoemitted electrons are measured with a 50 mm mean radius hemispherical electron analyzer operated at a 0.15 eV energy resolution and a

2° angular resolution. The analyzer (VSW HA50) is mounted on a double goniometer and can be tilted with respect to the sample in two independent directions. The AlN/SiC samples were fastened with tantalum wire to a molybdenum sample holder. The sample holder is biased by up to 4 V to allow low energy electrons to overcome the work function of the analyzer. The Fermi level of the system (sample and analyzer) is determined by UPS measurement of the sample holder with no sample bias (i.e., grounded). The sample holder can be heated to 1150 °C.

C. Results and Discussion

The UPS measurements were carried out on the AlN/SiC sample as loaded, and after anneals of 700 °C and 1000 °C. Auger Electron Spectroscopy (AES) and Low Energy Electron Diffraction (LEED) were also performed on the sample as-loaded, and after the anneals. The UPS data for the as-loaded AlN/SiC sample are displayed in Fig. 2. The spectra were obtained with different sample bias to overcome the workfunction of the analyzer. In the figure, all spectra have been displaced by the applied bias so that the Fermi level aligns. Two aspects indicate the presence of the NEA. The first is the detection of a low energy peak clearly observable with a sample bias of 3.0 Volts, with onset occurring at a bias of 1.5 Volts. The two low energy peaks of roughly the same height present at the 3.0 Volt bias are attributed to the normal secondary emission typical of UPS while the low energy feature is

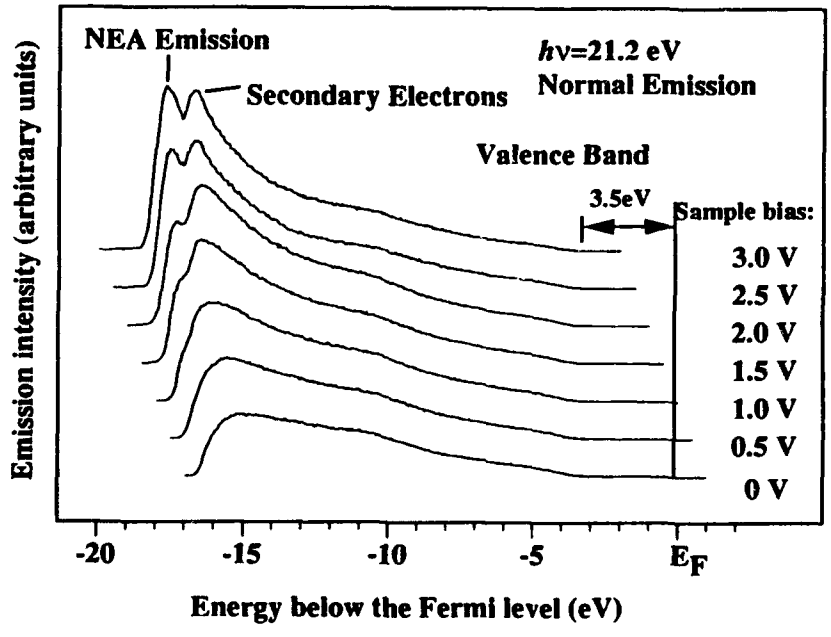

Figure 2. The uv-photoemission of AlN on 6H-SiC. The spectra were obtained at different sample bias to overcome the workfunction of the electron analyzer.

attributed to electrons thermalized to the conduction band minimum. This second peak is considered as the NEA peak since the electron count drops off so quickly. The large (~3V) bias is needed because the workfunction of the AlN is apparently less than that of the analyzer. The analyzer workfunction is between 4 and 5 eV.

The second indication of the NEA is that the widths of the photoemission spectra are consistent with the model described in Fig. 1. Here the width $W = h\nu - E_g$ where W extends from the low energy limit to the valence band maximum. We have used this relation to determine the position of the valence band maximum in the spectrum obtained with a 3V bias. The low energy limit was determined by linear extrapolation of the back edge to zero intensity. Then using the band gap of AlN as 6.2 eV and the 21.2 eV photon energy, the valence band maximum should then occur at 15.0 eV above this limit. The vertical line labeled Valence Band was obtained in this way. As is evident from the spectra, the valence band emission extends to this energy. We also note that the results indirectly verify that the band gap of the AlN film is the same as the bulk value of 6.2 eV. As mentioned earlier, the Fermi level is determined from the onset of electron emission from a metal sample.

The effect of annealing in vacuum was explored. After annealing to 700 and 1000 °C the photoemission spectra showed a decrease in the relative intensity of the NEA related peak (Fig. 3). Auger Electron Spectroscopy (AES) of the as-loaded surface showed oxygen and carbon contaminates in addition to the Al and N signals. After an anneal of 700 °C the AES showed a small reduction of the oxygen and a similar scale increase in the surface carbon, a trend that continued with the 1000 °C anneal. A LEED pattern was not visible from the sample as loaded or after the anneals of 700 °C and 1000 °C. We note that after a short H-plasma clean a faint 1×1 pattern was visible with an electron beam energy of 80 eV and the C signal was removed. The lack of a LEED pattern for the as-loaded and the annealed samples is possibly related to the carbon and oxygen on the surface. The reduction of the NEA related features indicates that the effect is related to the surface structure and termination of the AlN.

The second sample investigated was capped with a thin (<10Å) layer of silicon to prevent oxidation during transit. While the processing parameters were similar [14], the photo-emission spectra were different as can be seen in Fig. 4. A peak sharper than that of the NEA surface in Fig. 2 appeared with a bias of 3.0 Volts, but the width of the spectra was not consistent with the known band gap. As such ,we do not believe this to be a NEA surface. We attribute this to the presence of the silicon. Even after two plasma exposures, one of which was a deep etching exposure, we were unable to remove all of the silicon.

In comparison to the UPS spectra obtained from diamond surfaces which exhibit a NEA, [3-8] the feature in diamond is significantly sharper than that observed here for the AlN. There are several possible causes that could contribute to a broader signature. These could be

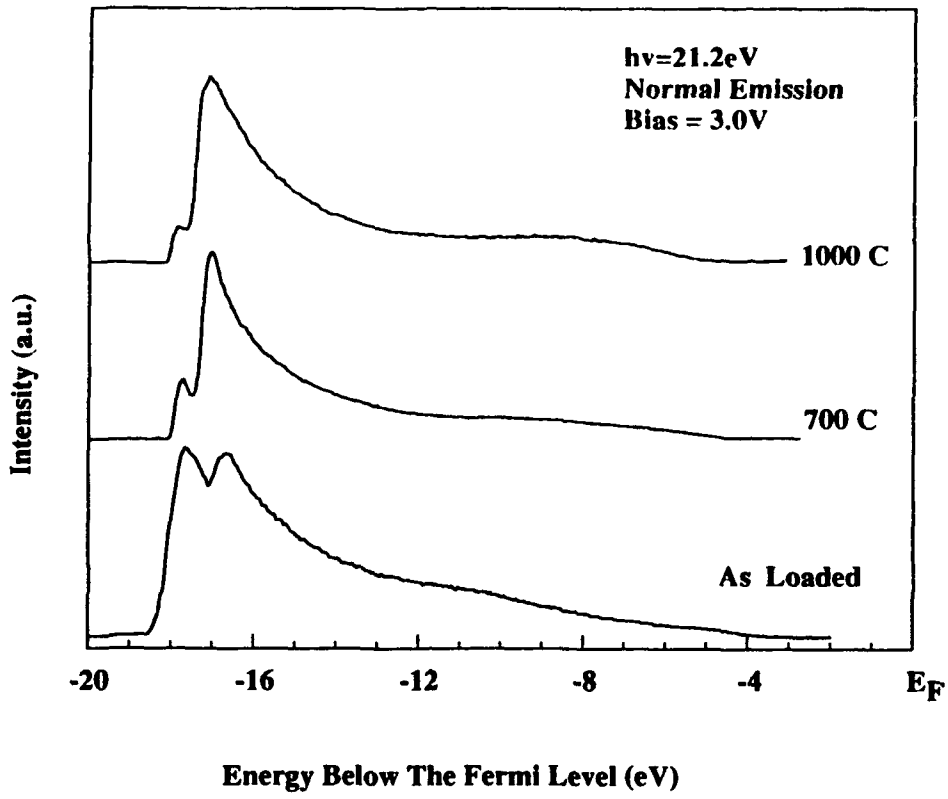

Figure 3. The uv-photoemission spectra of AlN on 6H-SiC as-loaded and after vacuum annealing at the indicated temperatures. All spectra were obtained with a sample bias of 3.0 kV.

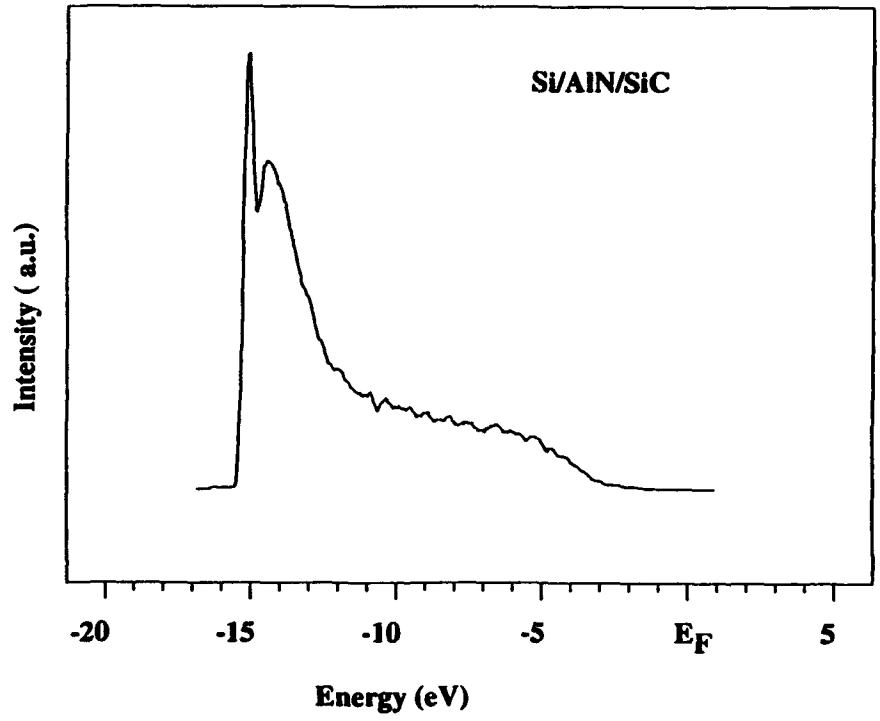

Figure 4. The uv-photoemission spectra of the second AlN on 6H-SiC sample studied. This spectrum was obtained with a sample bias of 3.0 kV.

related to a more disordered surface or to the intrinsic properties of the AlN (e.g., direct bandgap). Future research will explore these issues.

The last point that we address in this report is the position of the Fermi level in the AlN. From Fig. 1, it is evident that the surface Fermi level occurs at ~3.5 eV above the valence band maximum. This is near the center of the 6.2 eV bandgap. From this data we suggest a possible band alignment of AlN and SiC. Here we have assumed that there is no band bending in the AlN or in the SiC near the interface. Because of the wide band gap of the AlN, it seems unlikely that there is significant band bending in the thin film. The bulk Fermi level of the SiC has been determined from the doping level of the substrates to be ~0.3 eV below the SiC conduction band edge[12]. The results are summarized in Fig. 5. The band offsets are -0.8 eV at the valence band and 2.4 eV at the conduction band. The largest uncertainty in this proposed band offset is probably in the band bending in the SiC. Such band bending would result in an increase in the magnitude of the valence band offset and a decrease in the conduction band offset. While we are not aware of any calculations of the heterojunction band offsets of wurtzite AlN on 6H-SiC, there has been a calculation of the offsets of the (110) interfaces of cubic AlN/SiC [13]. The theoretical results also indicate a type I offset with band discontinuities of 1.5 eV at the valence band and -1.2 eV at the conduction band. This is qualitatively similar to the results presented in Fig. 5.

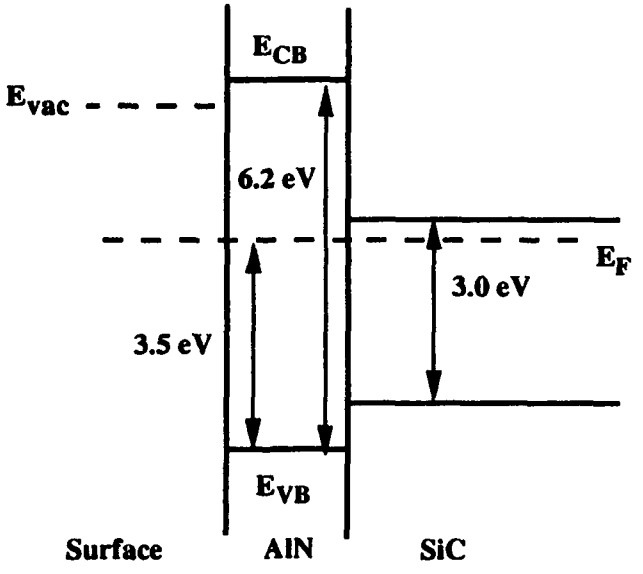

Figure 5. A schematic of the possible band alignment of AlN on 6H-SiC. The text describes the assumptions and related measurements.

D. Conclusions

In summary, we have observed features in the UPS spectra indicative of a NEA surface on as-loaded and annealed AlN on SiC. The measurements were made possible by the development of MBE heteroepitaxial growth of AlN on 6H-SiC. The NEA features are dependent on surface processing. The surface Fermi level of the AlN is found to be ~3.5 eV above the valence band maximum, and we have suggested a model for the band offsets assuming no band bending.

E. Future Plans

The preparation of the AlN films will be studied to determine the effect on the observed NEA. The aim will be to understand what parameter in the process has the greatest effect on the electron affinity. We will seek to understand if the observed behavior is latent or due to a surface contaminant lowering the workfunction. Films of various thicknesses will be studied.

F. References

1. J. H. Edgar, J. Mater. Res., **7**, 235 (1992)
2. H. S. Kong, J. W. Palmour, J. T. Glass, and R. F. Davis, Appl. Phys. Lett. **51**, 442 (1987)
3. C. Wang, R. F. Davis, Appl. Phys. Lett. **63**, 990 (1993).
4. M. D. Williams, M. D. Feuer, S. C. Shunk, N. J. Sauer, and T. Y. Chang, J. Appl. Phys. **71**, 3042 (1992).
5. F. J. Himpsel, J. A. Knapp, J. A. van Vechten and D. E. Eastman, Phys. Rev. B **20**, 624 (1979).
6. B. B. Pate, Surf. Sci. **165**, 83 (1986).
7. B. B. Pate, M. H. Hecht, C. Binns, I. Lindau and W. E. Spicer, J. Vac. Sci. Technol. **21**, 364 (1982).
8. J. van der Weide and R. J. Nemanich, J. Vac. Sci. Technol. B **10**, 1940 (1992).
9. J. van der Weide and R. J. Nemanich, Appl. Phys. Lett. **62**, 1878 (1993).
10. J. van der Weide and R. J. Nemanich, Phys. Rev. B15 **49** 13629 (1994).
11. Z. Sitar, M.J. Paisley, D. K. Smith and R. F. Davis, Rev. Sci. Instrum.. **61**, 2407 (1990).
12. J. Pelletier, D. Gervais, and C. Pomot, J. Appl. Phys. **55**, 994 (1983)
13. W. R. L. Lambrecht and B. Segall, Phys. Rev. **B43**, 7070 (1991).
14. L. B. Rowland, R. S. Kern, S. Tanaka, and R. F. Davis, in *Proceedings of the Fourth International Conference on Amorphous and Crystalline Silicon Carbide*, edited by C. Y. Yang, M. M. Rahman, and G. L. Harris (Springer, Berlin, 1992) p. 84.

V. Chemistry, Microstructure, and Electrical Properties at Interfaces between Thin Films of Cobalt and Alpha (6H) Silicon Carbide (0001)

Manuscript Submitted

to

Journal of Materials Research

for

Consideration for Publication

by

L. M. Porter and R. F. Davis

Department of Materials Science and Engineering, North Carolina State University, Raleigh, NC 27695-7907.

J. S. Bow, M. J. Kim, and R. W. Carpenter

Center for Solid State Science, Arizona State University, Tempe, AZ 85287-1704.

Abstract

Thin films (4–1000Å) of Co were deposited onto n-type 6H-SiC (0001) wafers by UHV electron beam evaporation. The chemistry, microstructure, and electrical properties were determined using x-ray photoelectron spectroscopy, high resolution transmission electron microscopy, and I-V and C-V measurements, respectively. The as-deposited contacts exhibited excellent rectifying behavior with low ideality factors and leakage currents of $n<1.06$ and 2.0×10^{-8} A/cm^2 at -10 V, respectively. After annealing at 1000°C for 2 min., the contacts showed ohmic-like character. Under the latter conditions significant reaction occurred resulting in the formation CoSi and graphite.

I. Introduction

The extreme thermal, mechanical, and electronic properties of SiC make it an attractive material for use in both structural applications and high-power, -temperature, -speed, and -frequency electronic and optoelectronic devices. The Co/SiC system has been studied by several investigators for the applications of both structural composites and contacts for devices[1-5]. Cobalt was reported to be a good rectifying contact on n-type 6H-SiC (0001) both in the as-deposited condition and after annealing at temperatures to 800°C, while ohmic-like behavior was displayed after annealing at 900°C[4,5]. Because Ni is commonly employed as an ohmic contact to n-type SiC[6], one also might expect ohmic behavior from annealed Co contacts when considering their chemical similarities and their similar work functions.

In this study, high resolution transmission electron microscopy (TEM) has been employed to investigate the interfacial chemistry and microstructure between Co and n-type 6H-SiC (0001) before and after annealing at 1000°C. The results of these studies have been compared with other chemical studies and correlated with the electrical properties measured in the present research.

B. Experimental Procedure

Vicinal, single crystal, nitrogen-doped, n-type ($\approx 10^{18}$ cm^{-3}) wafers of 1" diameter 6H-SiC (0001) containing 0.5-1.5 μm thick, n-type ($\approx 10^{16}$–10^{17} cm^{-3}) homoepitaxial films thermally oxidized to a thickness of 500–1000Å in dry oxygen at 1300°C were provided by Cree Research, Inc. The epitaxial layers were unintentionally-doped except where higher doping concentrations were needed; these latter films were intentionally doped with nitrogen during growth. The Si-terminated (0001) surface, tilted 3°–4° towards $[11\bar{2}0]$ was used for all depositions and analyses.

The substrates were simultaneously cleaned and the oxide layer etched from the surface using a 10 min. dip in a 10% hydrofluoric acid solution. This was followed by a quick rinse in deionized water. The substrates were loaded immediately into a vacuum system transfer tube (base pressure $\approx 10^{-9}$ Torr), thermally desorbed at 700°C for 15 min. to remove any residual hydrocarbon contamination, and transferred to the metal deposition chamber.

A UHV, dual source 270°, 10 cc electron beam evaporator was used to deposit the Co films in a thickness range of 4–1000 Å. A 330 l/s turbomolecular pump was used for roughing the system and during processing. A 500 l/s diode ion pump and a titanium sublimation pump were employed to achieve and maintain UHV base pressures of $<2\times10^{-10}$ Torr. Prior to the depositions, approximately 25–50 Å was typically evaporated from the source to liberate any foreign material which may have collected on its surface. Each substrate was covered by a shutter during this operation. To commence the deposition,

the emission current was increased very slowly until a deposition rate of 10–12 Å/min was stabilized according to the thickness monitor, and the shutter subsequently removed from in front of the sample. The pressure during the depositions was between 5×10^{-9} and 5×10^{-8} Torr. Throughout each deposition the substrates were rotated to ensure uniform thickness across the sample. The substrates were not intentionally heated during the depositions.

Patterned contact structures consisting of 500 μm (0.02") and 750 μm (0.03") diameter circular contacts of 100 nm thickness were created for electrical characterization by depositing the metal through a Mo mask in contact with the substrate. Silver paste served as the large area back contact. Subsequent annealing was conducted either in UHV or in an inert gas (N_2 or Ar) ambient. Current-voltage (I-V) measurements were taken with a Rucker & Kolls Model 260 probe station in tandem with an HP 4145A Semiconductor Parameter Analyzer. Capacitance-voltage (C-V) measurements were taken with a Keithley 590 CV Analyzer using a measurement frequency of 1 MHz.

Co/SiC samples were prepared in cross-section for analysis by transmission electron microscopy (TEM). High resolution (HR) images were obtained with an ISI EM 002B operating at 200 kV with an interpretable resolution limit of 0.18 nm. These images were typically recorded at an electron-optical magnification of 590,000. Lattice spacings (d-spacings) and interplanar angles were measured from optical digital diffraction patterns and used to identify the reaction product phases. The values of the lattice spacings of unknown phases were calculated using the (0006) d-spacing in 6H-SiC near the phase to be identified to avoid d-spacing errors introduced by changes in objective lens current. The experimentally-determined d-spacings were compared to a data base of d-spacings for each possible reaction product phase. The interplanar angles of the phases having d-spacings in the data base which were within 2% of the measured values were also compared for additional assistance in the identification. Most of the measured values were within 1% of the theoretical values. Unknown phases were identified uniquely by these procedures.

Analytical electron microscopy was performed using a Philips 400 ST FEG attached to a Gatan 666 parallel electron energy loss spectrometer (PEELS) operating at 100 kV and with a spatial resolution of approximately 3 nm. For fixed position PEELS the probe position was adjusted in the diffraction mode by monitoring the shadow image in the Bragg disk of the transmitted beam. The image was created by defocusing the second condenser lens. A liquid nitrogen cooled double-tilted holder was used for all analytical experiments to minimize specimen contamination.

Surface chemistry was studied using a Riber x-ray photoelectron spectroscopy (XPS) system. This system consists of a Mac2 semi-dispersive electron energy analyzer and is accessible by UHV transfer from the deposition chamber. The Mg Kα (1253.6 eV) x-ray

source was operated at 14 kV with an emission-controlled current of 15 mA. Scans of individual photoelectron peaks were obtained at 0.8 eV resolution and contained 500-750 data points and a 20-30 eV binding energy range.

C. Results and Discussion

Electrical Properties. As-deposited Co contacts displayed excellent rectifying characteristics with consistently low ideality factors ($n < 1.06$) and typical leakage currents of 2.0×10^{-8} A/cm^2 at -10 V (Fig. 1). Figure 2 shows a representative semilogarithmic I-V plot. The linear region extends over > 4 decades of current. At higher voltages the current became limited by the resistance of the substrate, and the slope was reduced. Following the procedure outlined in Ref. [7], the average Schottky barrier height (SBH) calculated from the semilogarithmic I-V plots was 1.12 eV.

Capacitance-voltage measurements plotted as $1/C^2$ vs. V yielded straight lines over a 2 to 5 V range, as shown in Fig. 3. These plots allowed the SBH to be calculated from the equation

$$\Phi_B = V_i + \xi + \frac{kT}{q} - \Delta\Phi, \qquad (1)$$

where V_i is the voltage intercept; ξ is the energy difference between the conduction band minimum and the Fermi level in the bulk of the material; and $\Delta\Phi$ is the image force lowering. The extrapolated voltage intercept was -1.00 V, yielding a calculated SBH of 1.15 eV.

The SBH of thin, as-deposited Co films on SiC were also calculated from XPS analyses by comparing shifts in the C 1s and Si 2p binding energies before and after deposition of very thin metal films. The binding energies of the C 1s and Si 2p peaks were defined as the full widths at half maximum of the C-bound-to-Si and Si-bound-to-C portions of the peaks, respectively. Table I lists the corrected C 1s and Si 2p binding energies as a function of Co film thickness. According to Ref. [7], the initial band bending at the SiC surface was 284.30 eV minus 283.80 eV (C 1s), which is equal to 0.50 eV. After depositing 12 Å Co the C 1s and Si 2p binding energies were both reduced by 0.56 eV, which corresponds to an increase in band bending by the same amount. This data indicates that the SBH was approximately equal to 1.06 ± 0.1 eV.

Calculation of the C 1s and Si 2p reduced intensities as a function of Co thickness indicated that island growth occurred rather than layer-by-layer growth. The same procedure outlined in Ref. [7] for Ti contacts was used to determine the growth mechanism. For the hcp Co film (a = 2.507Å, c = 4.07Å), the thickness of one monolayer was taken to be 2.04Å for the calculations. Figure 4 shows that the C 1s and Si 2p intensities were significantly higher than the theoretical intensities for layer-by-layer growth and closer to those for island growth (assuming 50% coverage). Higher substrate intensities are expected for island growth

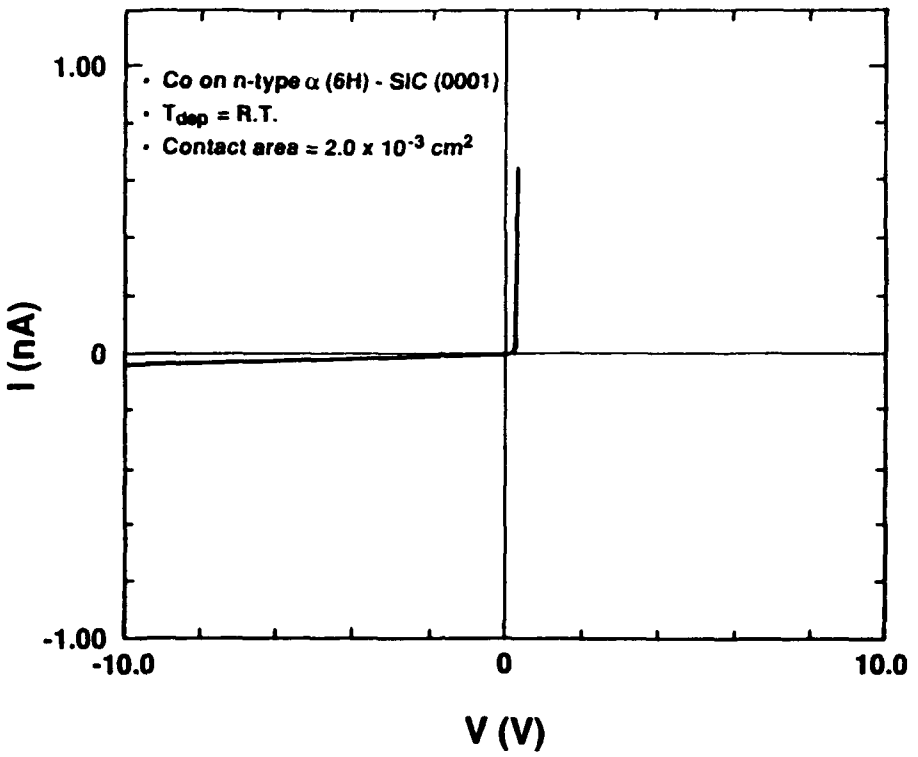

Figure 1. Representative plot of current-voltage data of as-deposited Co on 6H-SiC (0001).

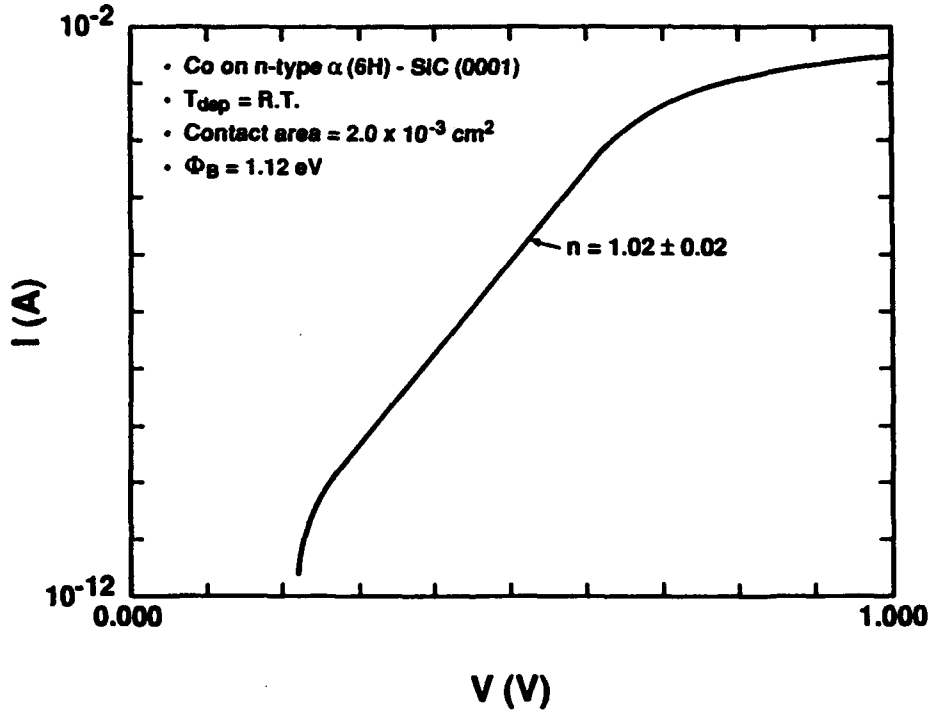

Figure 2. Semilogarithmic I-V plot of as-deposited Co on 6H-SiC (0001).

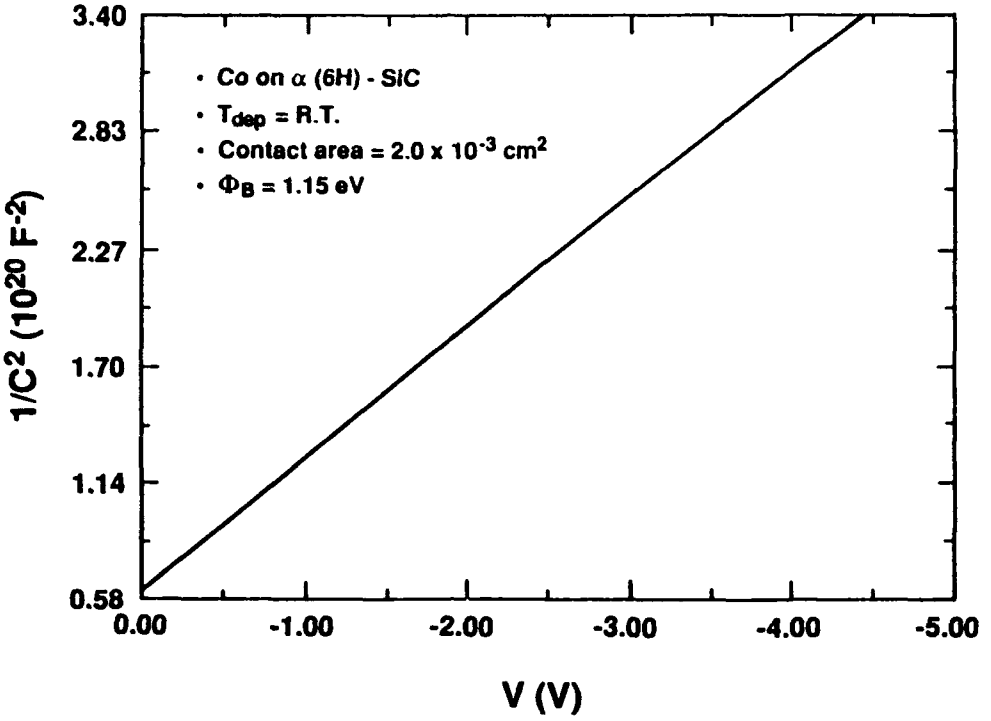

Figure 3. $1/C^2$ vs. V of as-deposited Co on 6H-SiC (0001).

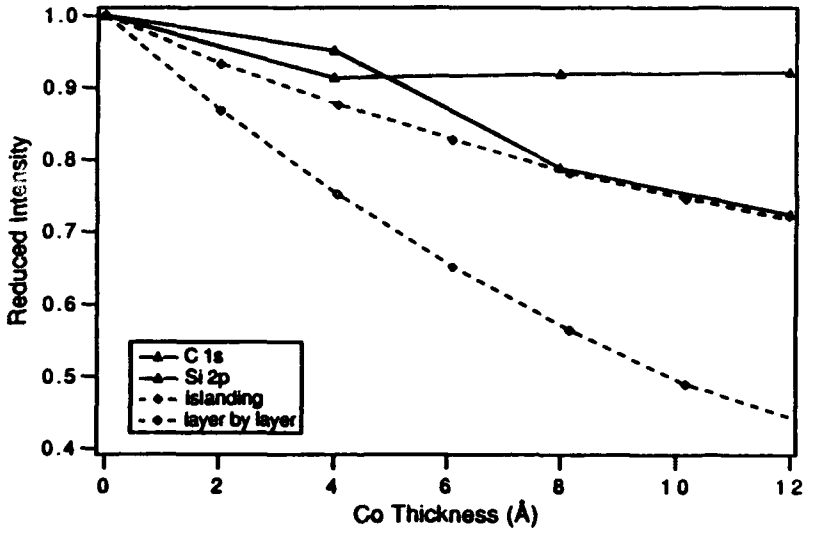

Figure 4. Plot of C 1s and Si 2p reduced intensities vs. Co overlayer thickness as measured by the growth thickness monitor. The theoretical curves represent island (Volmer Weber) growth, assuming 50% coverage, and layer-by-layer (Frank-van-der Merwe) growth.

Table I. Binding energies of C 1s and Si 2p peaks from SiC with various thicknesses of Co.*

Peak	0 Å Co	4 Å Co	8 Å Co	12 Å Co
C 1s	283.80	283.52	283.60	283.24
Si 2p	101.56	101.28	101.32	101.00

*These binding energies have been corrected according to the Au $4f_{7/2}$ binding energy. Units are in electron-volts.

because regions of the substrate are not covered by the deposited film. Therefore, less attenuation of the substrate peaks occurs. It is possible that complete coverage with thicker films would have resulted in more band bending in the SiC and, correspondingly, a larger calculated SBH. However, the close agreement between the values calculated from XPS and I-V and C-V measurements suggests that any change in that respect would be small. The islanding may be due to O in the film, which is discussed in a later section. The reason for the higher C 1s intensities compared to the Si 2ɔ intensities is unknown at this time.

Annealing of thicker films (1000Å) for 20 min. at 800°C resulted in an increase in the leakage currents by an order of 10^3 to 10^6. A few contacts displayed low ideality factors, while others displayed no linear region from which an ideality factor could be calculated. For the former the average SBH was 1.05 eV. However, the average SBH for all of the contacts was likely substantially lower than that.

Cobalt contacts were subsequently deposited onto another SiC substrate (epilayer carrier concentration of 9×10^{16} cm^{-3}) and rapidly annealed at 1000°C for total times of 1, 2, and 3 min. This higher temperature was chosen to determine whether ohmic behavior would result, as occurs in the Ni/SiC system[6]. The resulting electrical characteristics are displayed in Fig. 5. After 1 min. the contacts displayed very high leakage currents. No ideality factors could be obtained from the log I vs. V plots. After annealing for a total time of 2 min., the contacts became either ohmic or ohmic-like. However, in most cases, annealing for 3 min. resulted in an increase in the resistivity.

Because ohmic behavior was displayed after annealing for brief periods, Co was again deposited on SiC but through a Mo mask designed for TLM measurements. The SiC substrate was n-type with a carrier concentration of 3.4×10^{18} cm^{-3}. It contained a 3.0 μm thick, n-type homoepitaxial layer with carrier concentration 3.2×10^{18} cm^{-3}. This sample was also annealed for 2 min. at 1000°C. The average contact resistivity was $\rho_C = 2.5\ (\pm 0.4)\times10^{-2}\ \Omega\ cm^2$.

Microstructure. As-deposited Co films were mainly of the α-phase and polycrystalline, having a small angular range of orientations in the direction perpendicular to the substrate. In particular, $(0002)_{Co}$ is within ± 5° along $(0006)_{SiC}$. This orientation relationship is revealed

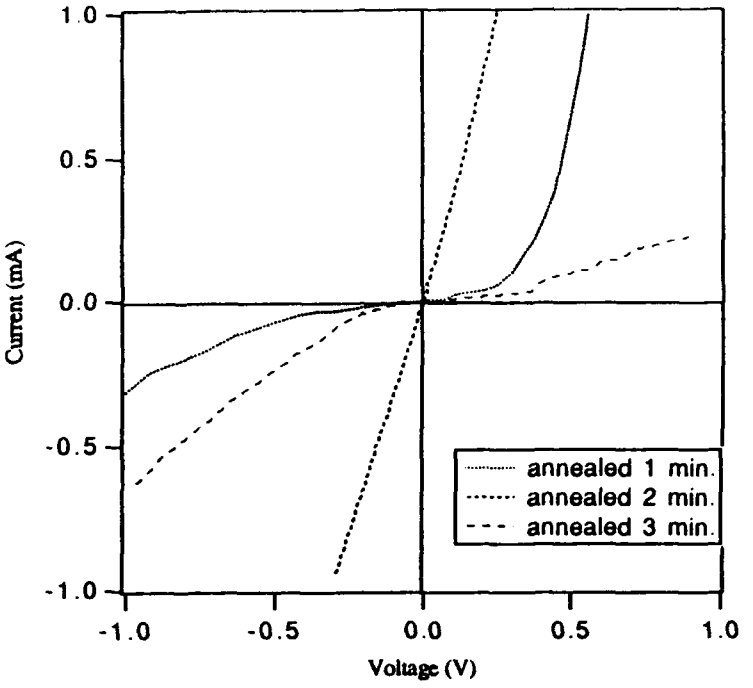

Figure 5. Current-voltage measurements of Co/SiC after annealing at 1000°C for 1, 2, and 3 min.

in the selected area diffraction (SAD) pattern in Fig. 6. A high resolution TEM image (Fig. 7) shows the high concentration of stacking faults in a representative film. An approximately 0.34 nm thick, white interfacial layer is apparent at the interface. This layer cannot be due to a new phase since the thickness is much less than the critical nucleation radius. The layer also is not attributed to ion milling damage during sample preparation, because its thickness remained constant across the sample, and no amorphous region in the Co or the SiC surrounded the layer. Considering the strain between the Co film and the SiC having the crystallographic relationship of $(0001)_{Co} \parallel (0001)_{SiC}$ to be as high as 18%, the white contrast is considered to be due to a local atomic density which is lower than the surrounding crystalline phases. Similar contrast for heterophase interfaces with large misfit strain has been reported in the literature[8,9].

Film Morphology & Phase Identification. Annealing the Co/SiC interface for 2 min. at 1000°C resulted in extensive reaction. Samples annealed under these conditions showed ohmic or ohmic-like behavior. Samples were also annealed at 800°C for 20 min., but did not produce ohmic contacts and were not analyzed by TEM. All of the Co (100 nm) and a thin layer of the SiC were consumed by the reaction at 1000°C. The low magnification TEM image in Fig. 8 shows the interface to be nonplanar, and, correspondingly, the width of the

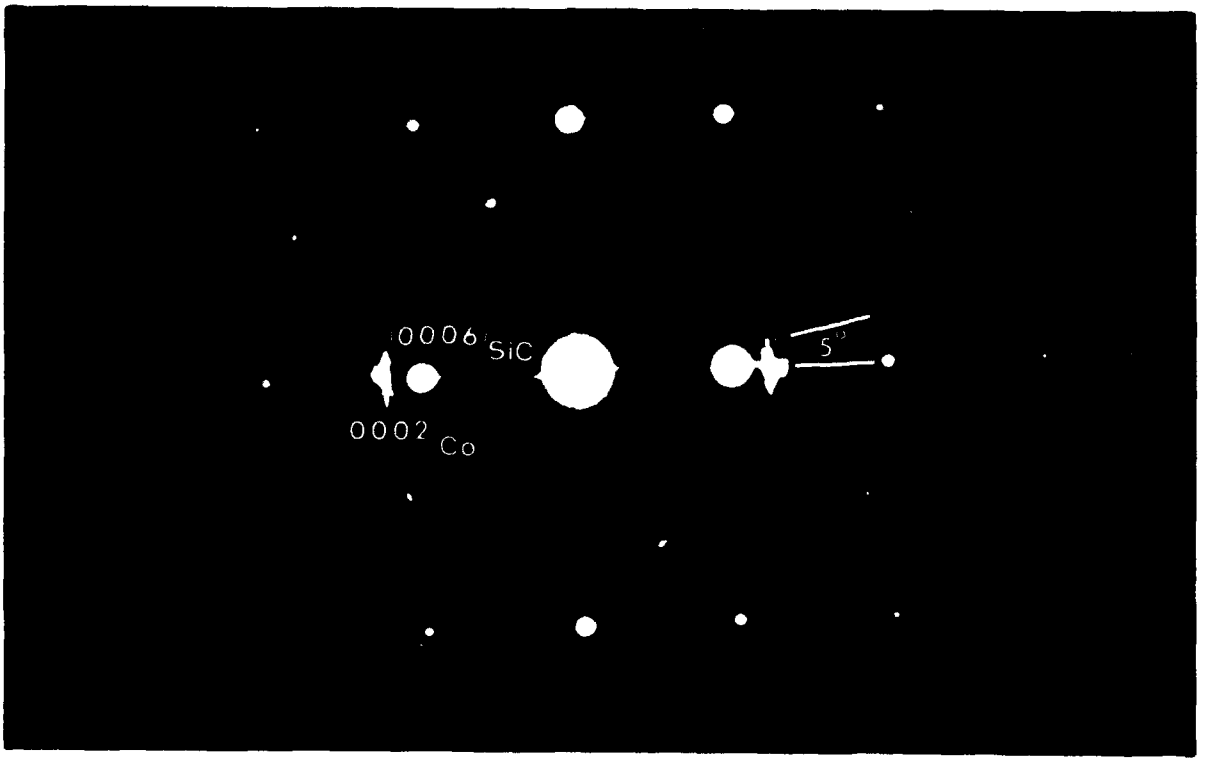

Figure 6. Selected area diffraction pattern of as-deposited Co on 6H-SiC (0001). Zone axis = $[1\bar{1}00]_{SiC}$.

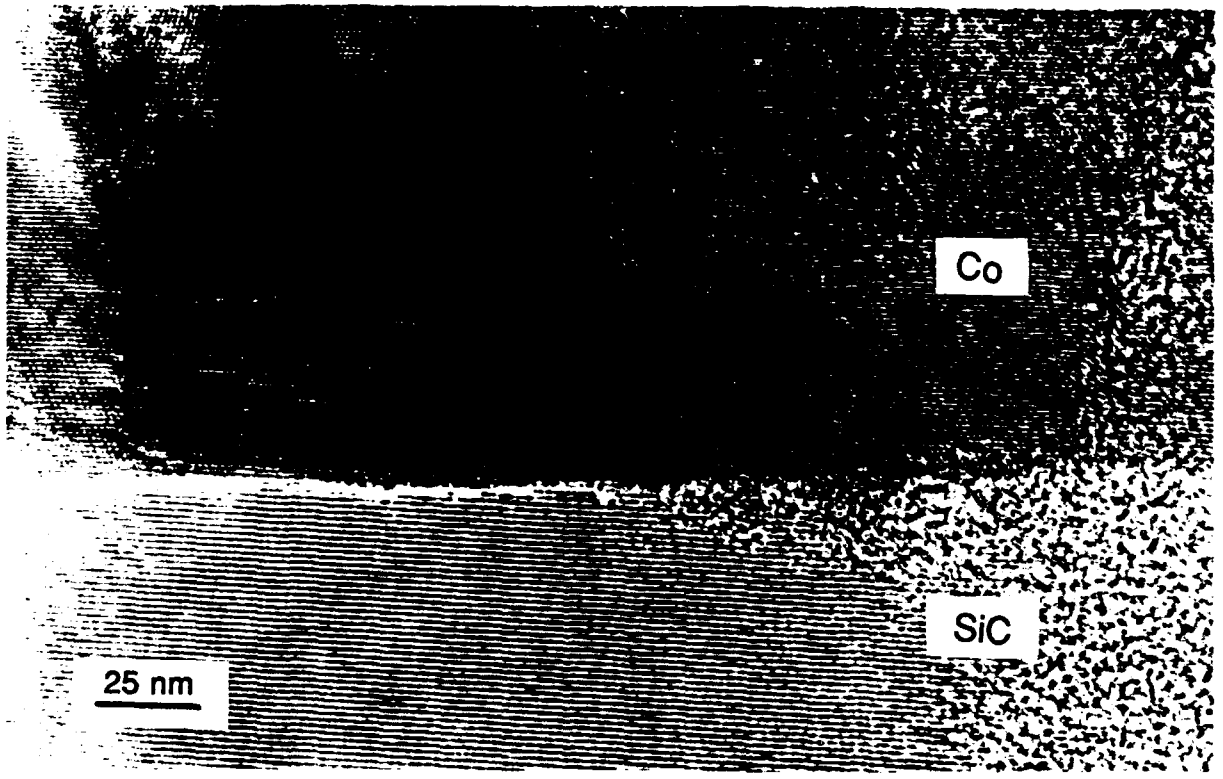

Figure 7. High resolution TEM image of as-deposited Co on 6H-SiC (0001) showing stacking faults in the film.

reaction zone varied. In fact, the narrow region of the reaction zone shown in Fig. 8 is approximately 200 nm, while the widest region is approximately 320 nm. The smooth, undulating interface morphology indicates that melting and solidification occurred during heating and cooling[1].

The reacted film may be divided into three layers according to Fig. 8. The layer adjacent to the SiC substrate is approximately 75 nm thick and is composed mainly of grains of crystalline phase(s) separated by low angle boundaries. Carbon aggregates displaying graphite fringes and which appear white in Fig. 8 are the dominant phase in the second layer. This layer is close to the original Co/SiC interface. Centered dark field (CDF) images, along with bright field (BF) images and PEELS data indicated that these aggregates were accompanied by voids.

The outermost layer contains a very long grain which is the same phase and has the same orientation to the grains in the first layer. A SAD pattern (Fig. 9) taken from this layer was indexed and the phase identified to be cubic CoSi viewed from the $[1\bar{1}2]$ zone axis. This phase also comprised the first layer, with the exclusion of one unidentified grain. The satellite spots along each main diffraction spot were attributed to double diffraction which resulted from grains with low angle grain boundaries along the electron beam path. Two orthogonal d-spacings measured from the SAD pattern and the microdiffraction pattern are 0.251 and 0.318 nm. They correspond to CoSi(111) (d = 0.2558 nm) and CoSi(110) (d = 0.3132 nm).

The higher magnification TEM image of the reacted interface in Fig. 10 shows a region of SiC protruding into the reaction zone. At the end of the protruded region, a small, faintly-observable region of SiC appears to be almost isolated from the SiC substrate. Selected area diffraction (SAD) patterns with rings corresponding to a d-spacing of 0.337 nm indicated the presence of graphite (d(0002) = 0.3362 nm). This and several other HRTEM micrographs revealed that graphite particles tended to contact these SiC protusions (see arrows in Fig. 10), probably to reduce the surface energy.

Nathan and Ahearn[3] studied the interface reactions between amorphous SiC (100 Å thick) and thermally evaporated thin films (50, 100, and 200 Å) of Ni and Co. A series of rapid anneals, corresponding to one temperature for each sample, was performed for 10 s at 25°C intervals between 300 and 450°C, 50°C intervals between 450 and 600°C, and 100°C intervals between 600 and 1000°C. At 1000°C samples were annealed for 60 s. After annealing the Co/SiC samples at temperatures between 400 and 600°C, Co_2Si was the only phase identified. After annealing at 1000°C, an uncertain phase, thought to be a crystalline C phase, and Co_2Si were present in the thicker samples. In the 50 Å films CoSi began to appear after 600°C annealing and higher.

In another study[1] diffusion couples were made between polycrystalline SiC, primarily β-SiC, and Pt, Co, and Ni. Before pressing the materials together the SiC and metals were

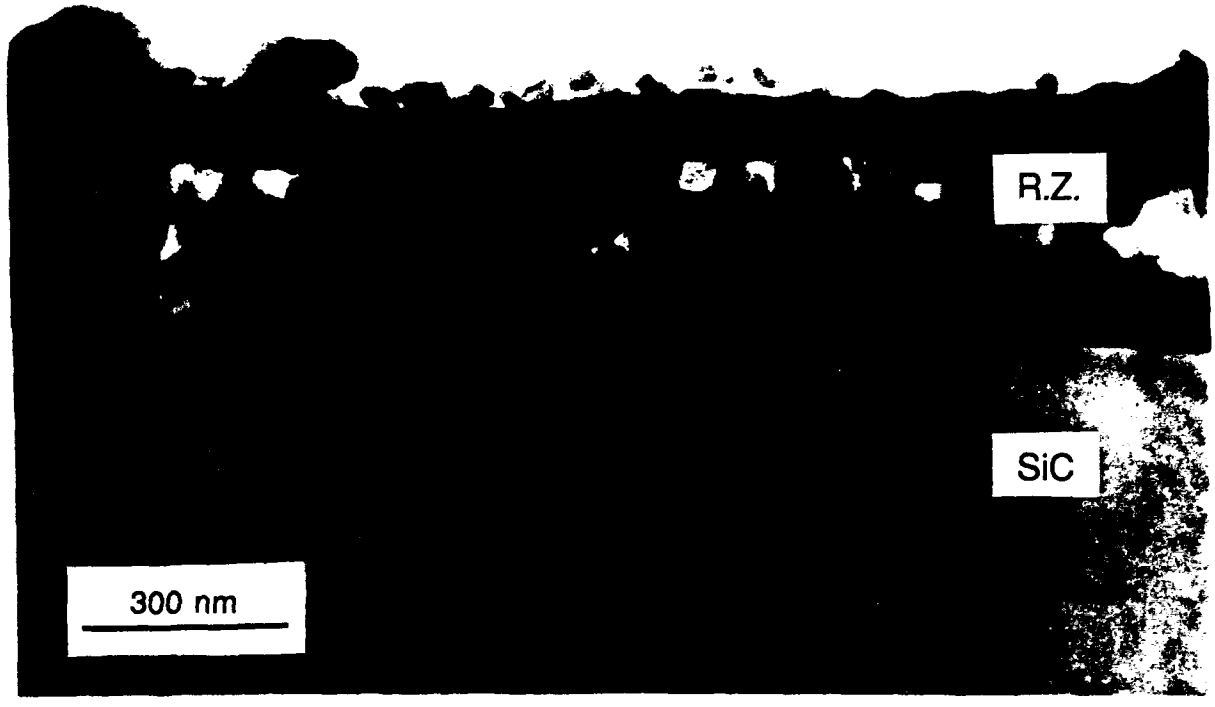

Figure 8. Low magnification cross-section TEM image of the Co/SiC interface after annealing at 1000°C for 2 min.

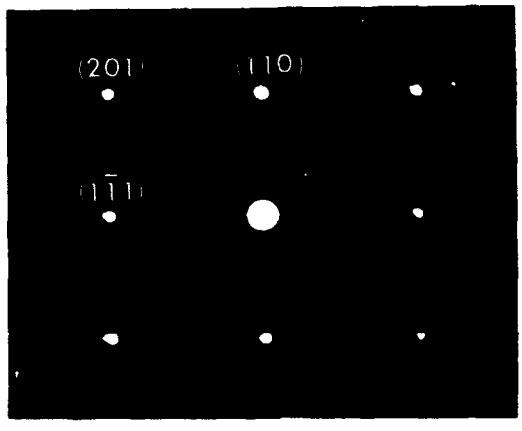

Figure 9. Selected area diffraction pattern from the outermost region of the Co/SiC reaction zone after annealing at 1000°C for 2 min. The pattern was indexed to be CoSi viewed from the [1$\bar{1}$1] zone axis.

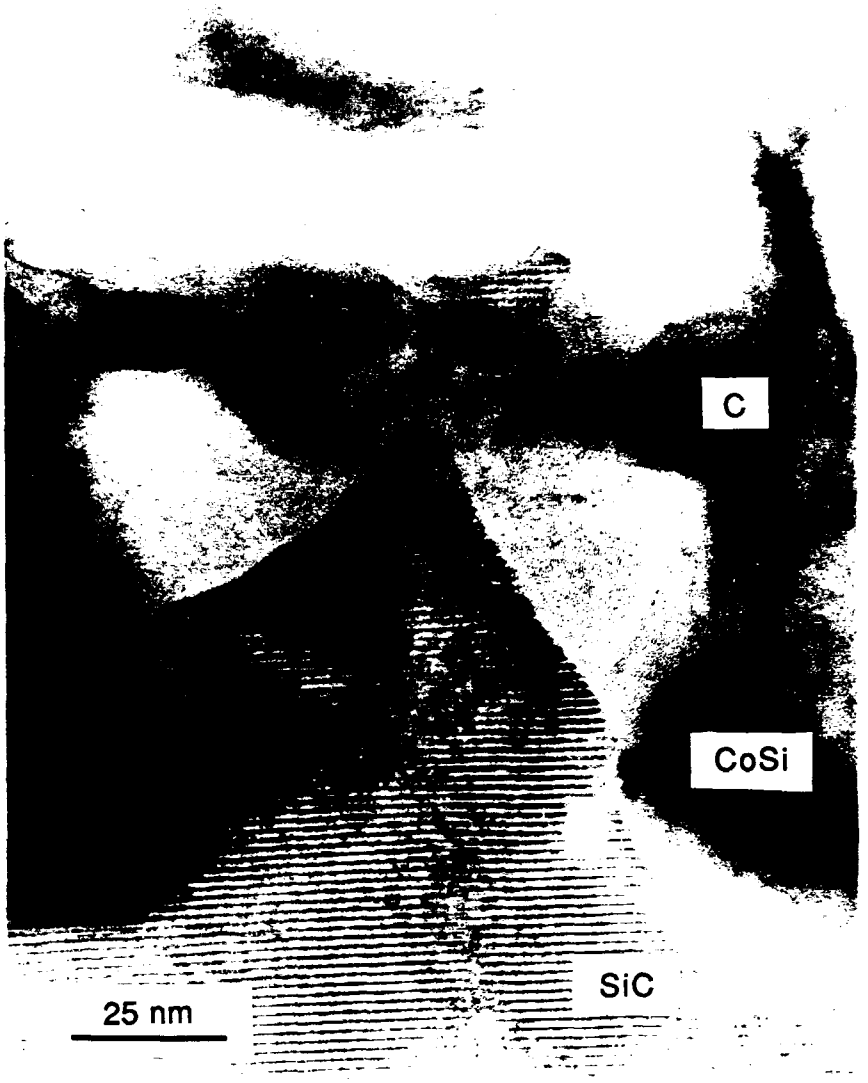

Figure 10. High resolution TEM image of Co/SiC reaction zone after annealing at 1000°C for 2 min.

polished, ultrasonically cleaned in acetone, rinsed in water, and dried with compressed air. After annealing at 1100°C for 6h, the Co/SiC reaction zone consisted of an ≈ 50 μm thick layer which contained both C precipitates and Co_2Si.

Comparing the present study with the other two studies discussed in the preceding paragraphs, it appears that Co_2Si forms in the Co/SiC system for thick and thin films of Co at temperatures between 400 and 1200°C when the Co film is not sufficiently thin as to limit the reaction. Because SiC has a very high bond strength, the initial stage of the reaction is

probably limited by the breaking of these bonds. However, once all of the Co has reacted to form Co_2Si, the evidence indicates that the reaction proceeds via the formation of CoSi.

Although CoSi was the phase in contact with the SiC after annealing for 2 min. at 1000°C, it is not believed to have inherent properties such as a low work function to cause the observed ohmic-like behavior. While the work function of CoSi (4.87 eV)[10] is less than that of Co (5.2 eV)[11], the difference should not be sufficient to account for the change. A potential future experiment would be to deposit CoSi on SiC without annealing and measure its electrical properties. Elemental doping from the contact layer, which could account for ohmic behavior, also is not likely to occur in this case. Because of the extensive reaction which resulted in highly nonuniform interfaces, it is likely that the post annealing electrical characteristics are associated with a high density of defects at the interfaces.

Interface Chemistry. Chemical bonding at the interfaces of thin, as-deposited Co films on SiC was studied with XPS. Both the C 1s and Si 2p peaks before and after depositing 4, 8, and 12 Å of Co are shown in Fig. 11. The C 1s peak of the uncoated SiC displayed only a Si-bound state, located at 283.80 eV. After depositing 4Å of Co, a small shoulder on the high binding energy side of this peak appeared. This shoulder grew substantially after depositing 8 and 12Å of Co. The higher binding energy indicates that the element with which the C is bound has a higher electronegativity than Si. There is no thermodynamically stable cobalt carbide. Moreover, the electronegativities of Co and Si are virtually identical; thus, Co-C bonding was ruled out as a possibility. In contrase, oxygen, has a very high electronegativity and forms oxides with Co which have large negative free energies of formation at room temperature (e.g. CoO (-214 kJ/mol) and Co_3O_4 (-795 kJ/mol)[12]). The O peak could not be monitored after depositing Co because the Co Auger peak interfered with the O 1s peak. Hydrocarbons, which are reported in the literature to have a C 1s binding energy of 285.0 eV[13], are another possible cause of the peak at higher binding energy. This peak would be expected to grow with increasing Co coverage as the photoelectron signal became more sensitive to interfacial C, and less sensitive to C within the bulk SiC material. This agrees with PEELS analysis which indicated O was present at a low level (~3 at. %) throughout the Co film.

The fact that no bonding states other than the Si-bound state were present in the C 1s peak from the clean SiC surface indicates that the O or hydrocarbons were introduced during the deposition process. It is not believed that these contaminants were introduced by a leak in the vacuum system (base pressure $1–2\times10^{-10}$ Torr) since they were not detected in other metal films, such as Ti, deposited in the same system. Also an Auger depth profile of the Co source revealed that O was not present at concentrations above the detection limit of the technique (1 at. %). Therefore, it is believed that the impurities were introduced either during the initial stages of the deposition or while transferring the sample through the vacuum system.

No Co silicide bonding was detected in the Si 2p peak, although three are known to exist in the Co-Si binary system[14]. Binding energies for Co-silicides were not found in the literature; however, Co-Si bonding would be expected to result in a peak at binding energies lower than the C-bound Si 2p peak. There was some evidence of enhancement of the minor O-bound Si 2p peak which was present before the deposition of Co.

D. Conclusions

A chemical, electrical, and microstructural study of as-deposited and annealed interfaces between Co and n-type 6H-SiC (0001) has been performed. The as-deposited contacts resulted in excellent rectifying behavior with low ideality factors ($n < 1.1$) and typical leakage currents of 2.0×10^{-8} A/cm^2 at -10 V. The SBH's calculated from XPS, I-V, and C-V measurements were between 1.06 and 1.15 eV.

After annealing at 800°C for 20 min., the contacts remained rectifying, but the leakage currents increased substantially. The contacts became ohmic-like after rapidly annealing at 1000°C for 2 min. HRTEM analyses revealed that the latter contacts were comprised of a mixture of CoSi and graphite. The reaction which formed these phases was extensive, consuming up to approximately 200 nm of the SiC. The ohmic-like behavior is likely due to defects created at the interface from the reaction.

E. Future Research Plans and Goals

The current technology of SiC devices is driving the need for ohmic contacts to p-type SiC which have low contact resistivities at both room and elevated temperatures. Aluminum alloys are currently used because the Al degeneratively dopes the surface of the SiC, which reduces the contact resistance. However, these contacts cause problems at elevated temperatures due to melting and extensive diffusion.

We are currently investigating three metal systems, one of which should be much more stable at elevated temperatures. The materials, which are comprised of 2-3 components, were chosen based on chemistry and doping considerations in addition to thermal stability. All three contact materials have been deposited onto p-type (and in one case n-type) 6H-SiC and have been characterized electrically after annealing at low-moderate temperatures.

Higher temperature anneals are planned for the contact material which has high thermal stability. For this system these temperatures are probably necessary to cause chemical reaction, which we believe will result in ohmic behavior. Once the preliminary studies involving annealing conditions and electrical properties have been performed, the chemistry and physics of these interfaces will be thoroughly investigated to understand the mechanisms related to the electrical behavior.

F. References

1. T.C. Chou, A. Joshi, and J. Wadsworth, J. Mater. Res., **6**, 796 (1991).
2. T.C. Chou, A. Joshi, and J. Wadsworth, J. Vac. Sci. Technol. A, **9**, 1525 (1991).
3. M. Nathan and J.S. Ahearn, J. Appl. Phys., **70**, 811 (1991).
4. N. Lundberg, C.-M. Zetterling, and M. Östling, Appl. Surf. Sci., **73**, 316 (1993).
5. N. Lundberg and M. Ostling, Appl. Phys. Lett., **63**, 3069 (1993).
6. G. Kelner, S. Binari, M. Shur, and J.W. Palmour, Electronics Letters, **27**, 1038 (1991).
7. L.M. Porter, J.S. Bow, R.C. Glass, M.J. Kim, R.W. Carpenter, and R.F. Davis, Submitted to J. Mater. Res.
8. K.L. Merkle, M.I. Buckett, and Y. Gao, Acta Metall. Mater., **40**, S249 (1992).
9. S.Q. Xiao, A.H. Heuer, and P. Pirouz, in *Proc. 50th MSA Annual Meeting*. 1992.
10. B.D. Wissman, D.W. Gidley, and W.E. Frieze, Phys. Rev. B, **46**, 16058 (1992).
11. C. Pirri, J.C. Peruchetti, G. Gewinner, and J. Derrien, Surf. Sci., **152-153, pt. 2**, 1106 (1985).
12. *JANAF Thermochemical Tables* Journal of Physical and Chemical Reference Data, (The American Chemical Society and The National Institute of Physics for the National Bureau of Standards, Midland, MI, 1985) Vol. 14, edited by M.W. Chase Jr., C.A. Davies, J.R. Downey Jr., D.J. Frurip, R.A. McDonald, and N.A. Syverud.
13. *Auger and X-ray Photoelectron Spectroscopy* 2nd ed. Practical Surface Analysis, (John Wiley & Sons, New York, 1990), Vol. 1, edited by D. Briggs and M.P. Seah
14. *Binary Alloy Phase Diagrams* 2nd ed. (ASM International, Materials Park, Ohio, 1990), Vol. 2 edited by T.B. Massalski, H. Okamoto, P.R. Subramanian, and L. Kacprzak.

VI. Distribution List

	Number of Copies
Dr. Yoon Soo Park Office of Naval Research Applied Research Division, Code 1261 800 N. Quincy Street Arlington, VA 22217-5660	3
Administrative Contracting Officer Office of Naval Research Resident Representative The Ohio State Univ. Research Ctr. 1960 Kenny Road Columbus, OH 43210-1063	1
Director Naval Research Laboratory ATTN: Code 2627 Washington, DC 20375	1
Defense Technical Information Center Bldg. 5, Cameron Station Alexandria, VA 22304-6145	2